

STUBBS, DAVID B. Ph.D. Disruption of Host Selenobiology by SARS-CoV-2 and Ebola Virus via RNA:RNA Antisense Interactions. (2023)
Directed by Dr. Ethan Taylor. 84 pp.

Selenium is an essential, but often overlooked, element in maintaining the health of our biological systems. Occupying the redox center of different selenoproteins, such as thioredoxin reductase (TXNRD) or glutathione peroxidase as selenocysteine (SeC), allows them to perform various unique biological functions, e.g., redox regulation and antioxidant defense. The synthesis of selenoproteins involves the reprogramming of a UGA stop codon to allow the recruitment of a SeC t-RNA. This occurs during translation, using a unique RNA structure called a selenocysteine insertion sequence (SECIS) element. The SECIS element can be located within the mRNA being translated but can also be hijacked from a second RNA molecule through antisense tethering. This tethering can also facilitate another translation event in the form of ribosomal frameshifting that allows genes to encode for multiple proteins by overlapping reading frames. Our research group has previously identified such frameshift sites in several pathogenic RNA viruses, including Ebola virus (EBOV) and HIV-1. This antisense tethering could enhance the frameshifting event to allow the recoding of those UGA codons as SeC. Evidence will be presented for these events being programmed in the genomes of EBOV and SARS-CoV-2. The EBOV nucleoprotein gene is an example of the reprogramming of a UGA stop codon as a potential SeC codon. Using green fluorescent protein as a downstream reporter gene, we show selenium-dependent read-through of the 3'-UGA stop codon, which is highly conserved only in the most virulent strains of EBOV. In the EBOV polymerase (L) gene, a programmed ribosomal frameshift signal leads to an overlapping gene with 2 tandem UGA codons immediately followed by an RNA region that is the inverse complement (antisense) to a region of the selenoprotein iodothyronine deiodinase II (DIO2) mRNA, which could both trigger the ribosomal frameshift

and provide access to the SECIS element contained in the DIO2 mRNA. We have designed an innovative assay for -1 frameshifting at such sites in which upstream and downstream reporter genes are used to assess the initiation and termination of protein synthesis. By inserting a wildtype or mutant viral insert, we show a highly significant level of -1 ribosomal frameshifting at the EBOV L gene site mentioned above. In SARS-CoV-2, we have demonstrated an antisense interaction between a region of the viral RNA and the mRNA for TXNRD3, another selenoprotein that is highly expressed in the human testes. This predicted antisense interaction was confirmed experimentally by knockdown of TXNRD3 mRNA in SARS-CoV-2 infected Vero cells. The significance of these findings regarding links between selenium status and the severity of Covid-19, and EBOV infection, will be discussed.

DISRUPTION OF HOST SELENOBIOLOGY BY SARS-COV-2
AND EBOLA VIRUS VIA RNA:RNA
ANTISENSE INTERACTIONS

by

David B. Stubbs

A Dissertation
Submitted to
the Faculty of The Graduate School at
The University of North Carolina at Greensboro
in Partial Fulfillment
of the Requirements for the Degree
Doctor of Philosophy

Greensboro

2023

Approved by

Dr. Ethan Taylor
Committee Chair

APPROVAL PAGE

This dissertation written by David B. Stubbs has been approved by the following committee of the Faculty of The Graduate School at The University of North Carolina at Greensboro.

Committee Chair

Dr. Ethan Taylor

Committee Members

Dr. Norman Chiu

Dr. Qibin Zhang

Dr. Jan Ruzicka

March 15, 2023

Date of Acceptance by Committee

March 15, 2023

Date of Final Oral Examination

TABLE OF CONTENTS

LIST OF TABLES	v
LIST OF FIGURES	vi
CHAPTER I: BACKGROUND	1
Introduction to Selenium.....	1
Selenium Incorporation and Stop Codon Readthrough	5
Programmed Ribosomal Frameshifting	7
Antisense Tethering Interactions	10
CHAPTER II: VALIDATED ANTISENSE TETHERING INTERACTIONS BETWEEN HOST SELENOPROTEIN AND VIRAL MRNAS	12
Introduction.....	12
Materials and Methods.....	13
Generation of Antisense Matches	13
Gel Mobility Shift Assays.....	14
Results.....	14
Discussion	21
CHAPTER III: SELENIUM-DEPENDENT READTHROUGH OF A 3'-UGA STOP CODON IN THE NUCLEOPROTEIN GENE OF EBOLA VIRUS.....	24
Introduction.....	24
Materials and Methods.....	25
Cell Culture	25
Engineering of GFP Expression Vectors Designed to Validate UGA Stop Codon Readthrough	26
Plasmid Propagation	26
Transfer of Viral Inserts to pAcGFP-N1 Plasmid.....	27
Transfection Protocol	27
Reporter Gene Assays	28
Results.....	29
Discussion	32

CHAPTER IV: A NOVEL RIBOSOMAL FRAMESHIFT SITE IN THE POLYMERASE GENE OF EBOLA VIRUS	34
Introduction.....	34
Materials and Methods.....	37
Frameshift Construct Design	37
Plasmid Propagation	39
Transfection Protocol.....	40
Reporter Gene Assays.....	40
Antisense Induction of Ribosomal Frameshifting in Dual Report Assay Construct	41
Results.....	42
Discussion.....	46
CHAPTER V: VIRAL MANIPULATION OF HOST SELENOBIOLOGY	48
Conclusions.....	48
REFERENCES	52
APPENDIX A: SUPPLEMENTAL TABLES AND FIGURES.....	63

LIST OF TABLES

Table 1. Fluorescent Reads of HEK Cells Transfected With Nucleoprotein Readthrough Construct.....	30
Table 2. Average Data From 7 Independent Experiments (A-G) Involving the Transfection of the Dual Reporter Frameshift Construct	43
Table A3. Sets A-G	64
Table A4. Antisense Induction of Frameshifting	71
Table A5. Amino Acid Sequence Homology of Copper Binding Proteins.....	72

LIST OF FIGURES

Figure 1. Correlation Between COVID-19 Cure Rate and Selenium Intake in 17 Cities Outside of Hubei, China	4
Figure 2. Mechanism of Recoding UGA Stop Codon as Selenocysteine via Stop-Codon Readthrough	6
Figure 3. Schematic of a -1 Ribosomal Frameshift in the HIV Gag-Pol Gene	9
Figure 4. Proposed Mechanism of Viral mRNA Capturing the SECIS Element of a Host Selenoprotein mRNA	11
Figure 5. Predicted Antisense Interactions Between Human Thioredoxin Reductase 3 mRNA (Red) and SARS-CoV-2 mRNA (Green) Forming RNA Duplexes.....	15
Figure 6. Predicted Secondary Structure of an Antisense Interaction Between Fruit Bat Thioredoxin Reductase 3 mRNA (Red) and SARS-CoV-2 mRNA (Green) Forming an RNA Duplex	16
Figure 7. Predicted Antisense Interaction Between Human Iodothyronine Deiodinase II mRNA (Red) and Zaire Ebola Virus Pol mRNA (Green) Forming an RNA Duplex	17
Figure 8. Gel Mobility Shift Assay Validating the Antisense Tethering Interaction Between Human Thioredoxin Reductase 3 DNA and SARS-CoV-2 DNA.....	18
Figure 9. Gel Mobility Shift Assay Validating the Antisense Tethering Interaction Between Fruit Bat Thioredoxin Reductase 3 DNA and SARS-CoV-2 DNA	19
Figure 10. Gel Mobility Shift Assay Validating the Antisense Tethering Interaction Between Human Iodothyronine Deiodinase II DNA and the Ebola Polymerase (L) DNA.....	20
Figure 11. Relative mRNA Levels of Thioredoxin Reductase Isoforms in Uninfected Cells (Blue) and SARS-CoV-2 Infected Cells (Red), Measured via Real-Time Polymerase Chain Reaction.....	22
Figure 12. Predicted Antisense Interactions Between Human Thioredoxin Reductase 3 mRNA (Red) and Ebola Nucleoprotein mRNA (Green) Forming RNA Duplexes	29
Figure 13. General Design of the Ebola Nucleoprotein Gene Readthrough Construct.....	29
Figure 14. Terminal 3' UGA Codon in the Ebola Nucleoprotein Is Recoded as Selenocysteine in HEK Cells.....	30
Figure 15. Selenium-Dependent Readthrough of UGA Stop Codon in Ebola Nucleoprotein Gene.....	31

Figure 16. Schematic of a Hypothetical Gene With a -1-Frameshift Site Leading to an Overlapping Gene Variant With an In-Frame UGA Codon That May Be Recoded as Selenocysteine	36
Figure 17. General Schematic of the Dual Reporter Frameshift Construct.....	39
Figure 18. Predicted Frameshift Site in the L Gene of Ebola Virus.....	42
Figure 19. Predicted Ribosomal Frameshift Site in the L Gene of Ebola Virus Using the KnotinFrame Program	42
Figure 20. HEK293T Cells Taken From an EVOS Fluorescent Microscope 2 Days After Transfection	43
Figure 21. Ratio of Green Fluorescent Protein to Luciferase Signals of Dual Reporter Assay Construct for the Validation of a Functional Frameshift Site	44
Figure 22. Ratio of Green Fluorescent Protein to Luciferase Signals of Dual Reporter Assay Construct After the Addition of Complementary Paired Sequences	45
Figure A23. Initial Construct Design Featuring Secreted Alkaline Phosphatase Upstream of the Potential Frameshift Insert.....	63
Figure A24. IntaRNA Results of DIO2 and Ebola L Gene From Figure 10.....	74
Figure A25. IntaRNA Results of SARS-CoV-2 and Fruit Bat TR3 From Figure 9	74
Figure A26. IntaRNA Results of SARS-CoV-2 and Human TR3 From Figure 8B.	75
Figure A27. RNAStructure Results of Ebola L Gene Oligo Used in Figure 10	76
Figure A28. RNAStructure Results of DIO2 Used in Figure 10.....	77
Figure A29. RNAStructure Results of Human TR3 Oligo Used in Figure 8.....	78
Figure A30. RNAStructure Results of SARS-CoV-2 Oligo Used in Figure 9	79
Figure A31. RNAStructure Results of SARS-CoV-2 Oligo Used in Figure 8	80
Figure A32. RNAStructure Results of Bat TR3 Oligo Used in Figure 9	81
Figure A33. Raw Uncropped Gel of Figure 8	82
Figure A34. Raw Uncropped Gel of Figure 9	83
Figure A35. Raw Uncropped Gel of Figure 10	84

CHAPTER I: BACKGROUND

Introduction to Selenium

Recent viral outbreaks across the world have renewed focus on the intimate relationship between us, the host population, and them, the microscopic pathogenic particles that have plagued us from time immemorial. With the global research that has gone into viral studies, we have gained a tremendous understanding of the viral mechanisms that underlie our own infections. A potentially critical component is, of course, nutrition, specifically the micronutrient catalogue that we must maintain with regularity alongside the other components of our diet. Of these, selenium is a vital element that is critical in viral infections not only for our own cells, but also for the pathogen.

Selenium is classified as a trace element in the human body and is maintained in the environment in most systems, such as soil, water, and atmosphere, and is mostly acquired by humans through diet or direct supplementation (Winkel et al., 2015). Its role as a trace element is unique in that it is directly coded for in our genome as the 21st amino acid selenocysteine (SeC), a modified version of the more abundant alcohol, serine (Rayman et al., 2022). Selenocysteine differs from the similar amino acid cysteine in that its functional selenol group has a lower pKa compared to a thiol group, resulting in ionization at physiological pH (Burk et al., 2003). This unique nature of this amino acid is reflected in the nomenclature of proteins possessing this residue, known as “selenoproteins” or “selenoenzymes.” Twenty-five of these selenoproteins have been discovered within our genome, functioning mainly in the redox centers of proteins involved in antioxidant function, maintaining redox homeostasis, anti-inflammatory responses, thyroid and immune cell function, and selenium transport (Zhang, Saad, et al., 2020) (Bellinger et al., 2009). In terms of redox function, only the tetravalent selenite form is used in the active

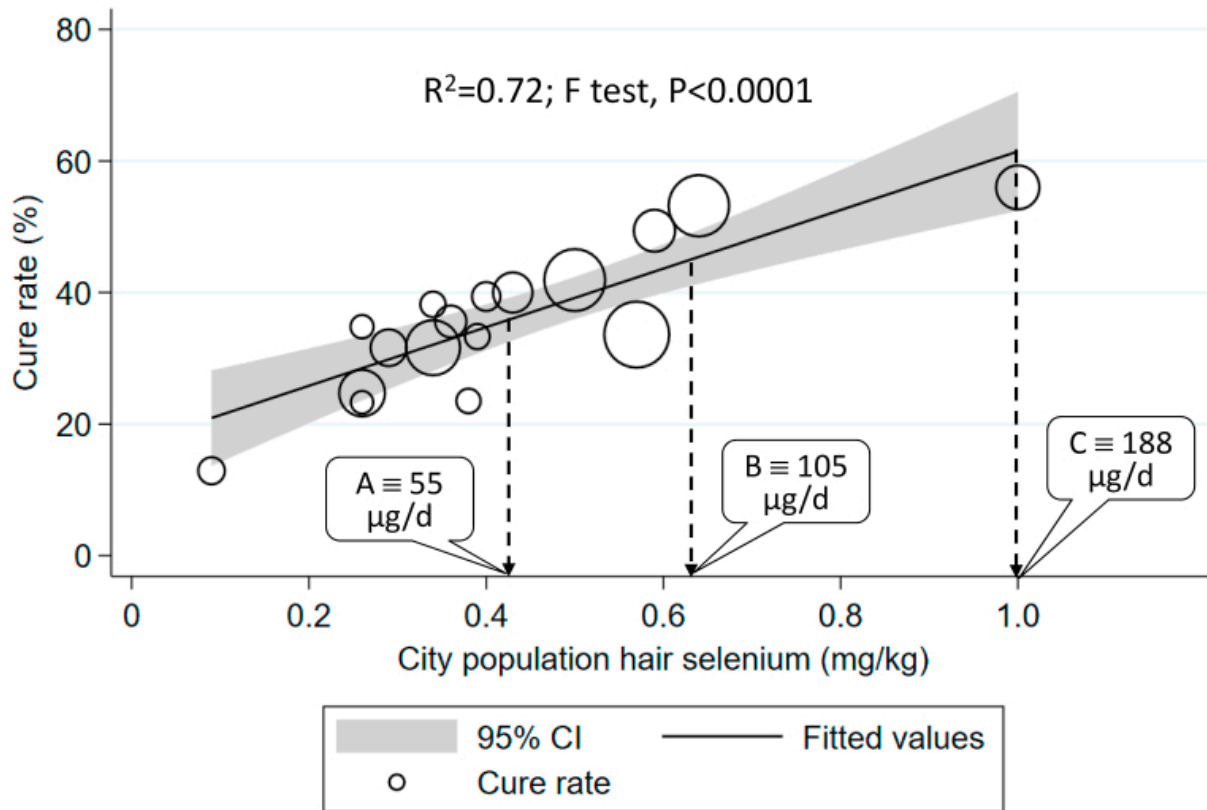
site of redox selenoproteins as opposed to the hexavalent selenate form (Lipinski, 2015). Redox proteins containing selenium benefit from this by having an increase in the catalytic rate constant at lower pHs, favoring selenoproteins for those oxidative stress functions (Burk et al., 2003).

Several noteworthy and relevant examples of selenoproteins include glutathione peroxidases (GPxs), which serve an immune function within oxidative stress protection through the conversion of lipid hydroperoxides to their alcohol forms, as well as converting free hydrogen peroxide to water (Brigelius-Flohé, 2006). It is also within the thioredoxin reductase (TXNRD) family, two of which serve redox homeostasis functions in the cytosol and mitochondria (TXNRD1 and 2), and a third of this family, TXNRD3. This enzyme reduces its namesake, thioredoxin, which is an important biological reducing agent, e.g., as part of the deoxyribonucleotide synthesis pathway (Z. Huang et al., 2012) (Yoshioka, 2015) (Holmgren & Sengupta, 2010). It is part of selenoprotein P (SELENOP) whose nomenclature arose from its staggering composition of SeC residues, where most selenoproteins contain a single SeC; this aptly named protein contains 10. This results in SELENOP being the major form of selenium in our bodies, secreted as a glycoprotein into blood plasma (Saito & Takahashi, 2002). Selenium is also a part of iodothyronine deiodinase II (DIO2), the principle enzyme involved in converting the prohormone thyroxine (T4) into its active form, triiodothyronine (T3), via outer ring deiodination (Luongo et al., 2019).

The recommended daily intake of this micronutrient is between 25 and 100 micrograms (Zhang, Saad, et al., 2020). While this may seem light compared to elements like iron (whose recommended daily intake is in the milligram range, several orders of magnitude higher), selenium's deficiency is not without concern, especially in a period of a viral epidemic (*Dietary Supplement Use in the United States, 2003–20061 | Elsevier Enhanced Reader, n.d.*).

Selenium's function in relation to viruses is quite important given its various roles in the immune system, where its deficiency has led to a downturn in immune function and antioxidant responses (Bermano et al., 2021) (Beck et al., 2003) (Stýblo et al., 2007). A decrease in selenoprotein antioxidant activity leads to an increase in reactive oxygen species that leads to an increased expression of proinflammatory cytokines (Heyland et al., 2005). A lack of selenium in viral infections has seen an increase in mutations (influenza), viral replication (hantavirus), and general virulence of the disease as it relates to morbidity (Ebola virus, Coxsackievirus B3 and Human Immunodeficiency Virus Type 1) (Gill & Walker, 2008) (Beck et al., 2003) (Nelson et al., 2001) (Fang et al., 2015) (Constans et al., 1995). With respect to replication and mutation rate, an increase in oxidative and nitrosative stress can increase the rate at which these can occur in viral genomes (Molteni et al., 2014). This is particularly relevant to RNA viruses, whose mutation rates are significantly higher than that of DNA viruses due to the RNA-dependent RNA polymerase lacking proofreading capabilities, which lead to a mutation per genome every replication cycle (Beck et al., 1995). Within the most recent epidemic, a study from China was conducted across several cities outside the province of Hubei, where a positive correlation was shown between the reported cure rate of SARS-CoV-2 and the concentration of selenium in hair, a relative measure of selenium intake (Figure 1) (Zhang, Saad, et al., 2020).

Figure 1. Correlation Between COVID-19 Cure Rate and Selenium Intake in 17 Cities Outside of Hubei, China



Selenium supplementation (usually in the form of sodium selenite) in an effort to treat illness has shown to be beneficial, even in response to sepsis (T.-S. Huang et al., 2013). Interestingly enough, a significant body of data regarding selenium supplementation comes from adjuvant therapy of RNA viral infections (Steinbrenner et al., 2015). An exception to this was found in China through trial studies with dietary selenium supplementation to find a decreased incidence of liver cancer in individuals infected with a DNA virus, Hepatitis B (Yu Yu et al., 1997).

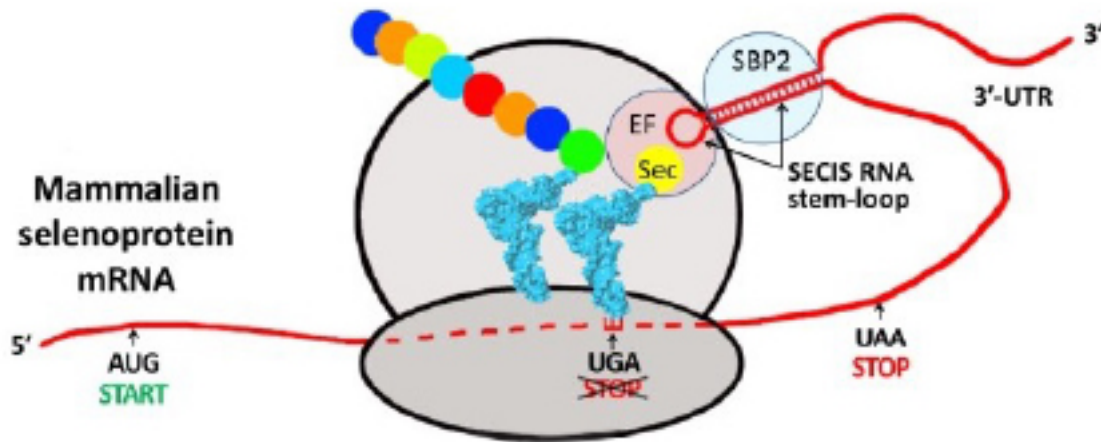
Selenium's further relevance to viral infections comes from selenoproteins encoded by the viral genome itself. A GPx homolog has been found in HIV that is potentially used for redox

regulation as oxidative stress is needed for replication (Zhao et al., 2000) (Israel et al., 1992). This nutrient's role in pathogenicity is not as well categorized as other nutrients, yet it still demands study due to potential relevance in various viral infections (Rayman et al., 2022).

Selenium Incorporation and Stop Codon Readthrough

Selenocysteine incorporation during peptide synthesis on the ribosome differs from other amino acids in that it is encoded by a UGA stop codon, usually responsible for recruiting termination factors to stop translation. The selenocysteinyl tRNA must be assisted by a series of recruitment factors such as SECIS Binding Protein 2 and an elongation factor specific to this mechanism, which allow the tRNA to bind to the A site as well as suppress the termination factor that is usually associated with the UGA stop codon. This whole process only occurs at a UGA located in an mRNA that contains a downstream selenocysteine insertion sequence (SECIS) element. This intramolecular 3D stem-loop structure is inherent to the mRNA being translated and forms downstream of a UGA stop codon, allowing the binding of the selenocysteinyl tRNA (Figure 2) (Gonzalez-Flores et al., 2013). There is evidence to suggest that the SECIS element may be derived elsewhere other than from the translated mRNA, which will be explored in subsequent chapters (Will Taylor et al., 2016). Despite a SECIS element being present downstream of a UGA codon, this process only occurs with low efficiency, between 5% and 10% of the time (Mehta et al., 2004).

Figure 2. Mechanism of Recoding UGA Stop Codon as Selenocysteine via Stop-Codon Readthrough



Note. The mammalian selenoprotein mRNA (red) contains a SECIS element that allows the translation of the UGA codon as SeC, which is added to the growing peptide instead of terminating translation. The protein then terminates at the next downstream non-UGA stop codon.

EF = elongation factor; SBP2 = SECIS binding protein 2.

Naturally, if a UGA stop codon is recoded into SeC, the translation process continues until the next stop codon is reached. This is an example of the more general phenomenon of stop codon readthrough.

Each UGA does not necessarily encode for a SeC, however. There are other mechanisms by which translation may not stop at a stop codon. Termination factors naturally cease translation at the location of the UGA codon, but if an aminoacyl tRNA were to recognize a UGA codon by having a mutated anticodon, then in that particular instance you would add a residue instead of terminating translation. This is the case with suppressor tRNAs (Herring & Blattner, 2004).

Viruses have used this phenomenon in the case of the murine leukemia virus where the

expression of the pol gene is dependent on readthrough of the preceding UAG codon from the gag gene. Though the insertion of a glutamine at that position only occurs roughly 5% of the time, the result is a near 1:20 ratio of pol to gag protein, which is suitable given the higher number of gag structural proteins needed compared to enzymes (Feng et al., 1992). Viruses need to take advantage of these kinds of mechanisms to enhance the efficiency of their own gene expression. Viruses have genomes much smaller than our own and need ways to consolidate information in order to survive (Cui et al., 2014). Stop codon readthrough allows for modulation and expression of multiple proteins without a separate site of ribosomal initiation.

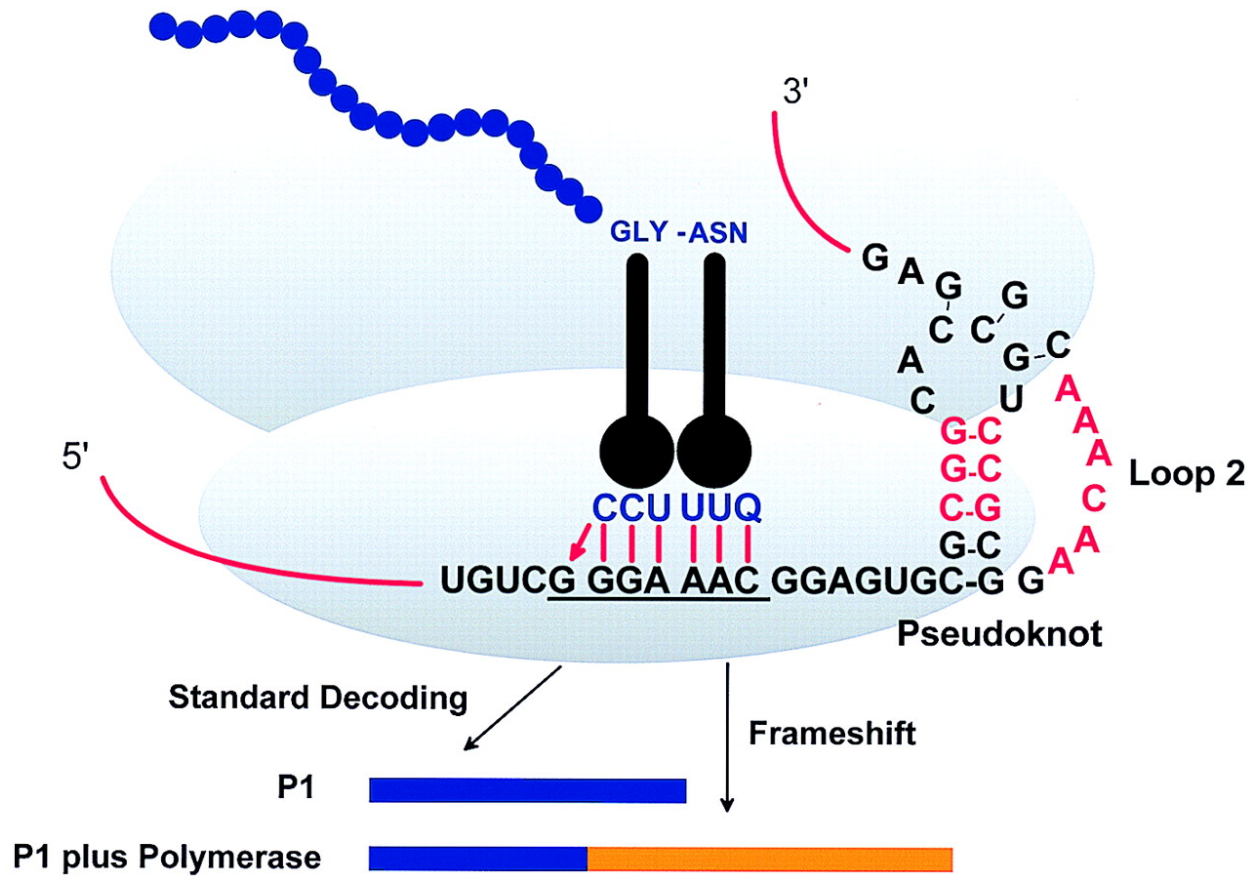
Programmed Ribosomal Frameshifting

Another mechanism by which viruses can condense the amount of information needed to propagate is ribosomal frameshifting. mRNA is read 3 bases at a time as triplets or codons in sequence that each code for an amino acid, ending at a codon that terminates the translation of that mRNA. The frame that this sequence covers, starting at an AUG start codon and ending at a stop codon, is referred to as the open reading frame (ORF). Multiple reading frames can exist within a single sequence by shifting forward or backward a single base from the reference frame or 0 frame; a new frame is entered with alternate coding potential (Brent, 2005). Shifting the read frame forward or backward by more than a single base is also known to rarely occur (e.g., +2 or -2 from the reference frame), or even via skipping over multiple bases via “ribosomal hopping” (Rogers et al., 1991). No single frame is necessarily the “correct” one, instead a single sequence should be thought of as having the potential to code for multiple proteins by containing multiple overlapping read frames.

During translation, the ribosome can move from one frame to another in a frameshift, which can happen accidentally, or be “programmed” for the deliberate purpose of encoding a

protein variant. This event occurs at specific sites in the mRNA, characterized as a “slippery” or “shifty” sequence, which in the case of -1 frameshifting, is ideally a heptamer with the motif X XXY YYZ in the 0 frame, where X is any base, Y A or U and Z is not G (Cao & Chen, 2008). This pattern allows the current A and P site aminoacyl-tRNAs to bond with the adjacent codon while maintaining proper codon-anticodon pairing. This is in part due to the flexibility of the “wobble” position in the codon, the last base that is varied in amino acid coding. A single amino acid will have several codons that differ at that position. For example, arginine is recognized by CGA, CGU, CGC, and CGG. This slippage can occur when the ribosome is stalled during translation, giving those anticodons time to potentially pair with a new triplet one base forward or back. This stalling can occur when a particular amino acid is at low enough cytosolic concentration that it takes time for one to be found, in which the second 0 frame codon is for a rare amino acid (Olubajo & Taylor, 2005), or from the formation of a downstream secondary structure called a pseudoknot (Green et al., 2008). This pseudoknot is yet another stem loop that can form from the mRNA being translated, separated from the slippery sequence by a 5-8 nucleotide spacer region (Lin et al., 2012). The pseudoknot typically forms from 2 stem loops, where the first loop forms part of the second stem (Green et al., 2008). These events occur in tandem to incur a frameshift (Figure 3).

Figure 3. Schematic of a -1 Ribosomal Frameshift in the HIV Gag-Pol Gene



Note: The mRNA is bound to the ribosome, with a pseudoknot formed downstream. The anticodons of glycine and asparagine are “slipping” back one base at the slippery sequence heptamer. Two potential products are shown at the bottom: P1 is the 0-frame product, where no frameshift occurs, and the bottom product occurs with a frameshift.

As with stop codon readthrough, the efficiency of this event is usually low—sometimes as low as 0.5%—but can be as efficient as 80% (Rodnina et al., 2020) (Atkins et al., 2016) (Advani & Dinman, 2016). This mechanism allows a virus to encode for multiple proteins via multiple overlapping reading frames within a single genomic sequence. The HIV gag-pol fusion protein, much like the murine leukemia virus, is expressed at a ratio of 20:1 relative to the gag protein. The pol gene is out of frame of the gag gene and is expressed only 5% of the time when

a frameshift occurs (Jacks, Power, et al., 1988). This is a useful mechanism used by many other viruses to condense information (Jacks, Madhani, et al., 1988).

Antisense Tethering Interactions

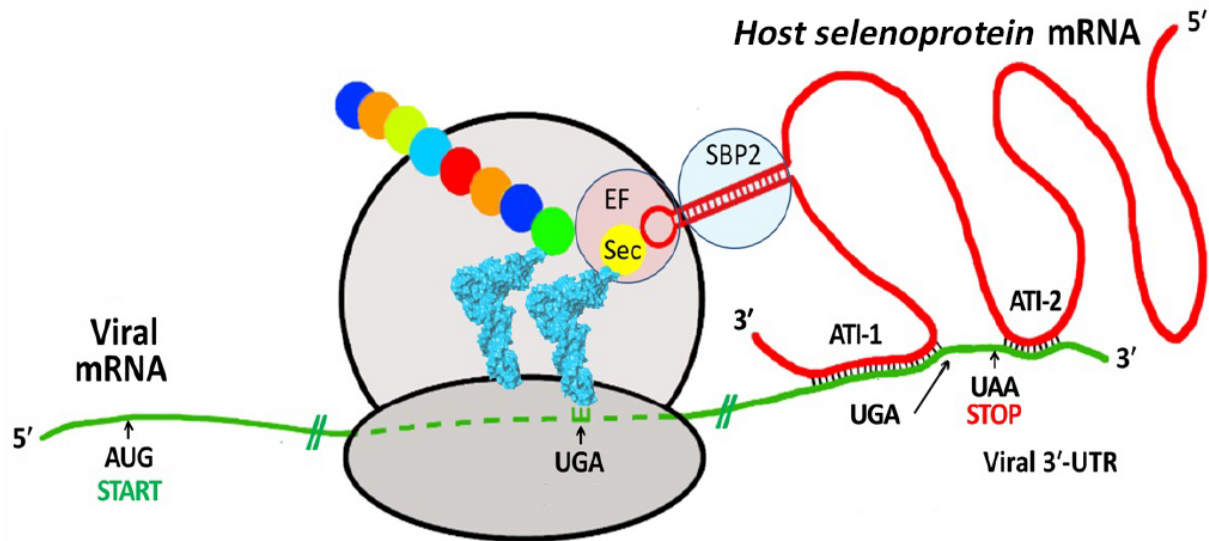
Both previous mechanisms involve reducing the amount of information that a virus would need to encode by effectively reducing the necessary bases to code for particular proteins. There exists the potential for further reduction by achieving the use of molecular functions without adding any extra bases: antisense tethering interactions (ATIs).

Nucleotides can maintain interactions within themselves and between each other based on their base sequence. DNA naturally occurs as double stranded, where the sense strands sequence is the reverse complement of the antisense strand. However, this extends further beyond genomic DNA; RNA sequences often form internal antisense interactions within themselves (e.g., the SECIS element stem loop and the ribosomal frameshift pseudoknot) and between each other (siRNAs or microRNAs). siRNAs and microRNAs usually lead to the degradation of target mRNAs, or at the very least, downregulation of that mRNA through the prevention of translation initiation or stalling the ribosome enough to terminate translation completely (Zeng et al., 2003).

This method of regulation requires sequences to have enough complementarity to maintain a duplex that is strong enough to overcome the bond energies of internal pairing. In many cases, RNA viruses have sequences that have significant complementarity to human mRNAs (Wang et al., 2021) (Taylor et al., 2016). Such antisense interactions can affect the knockdown of host mRNAs, but, additionally, viruses may use an antisense interaction to capture a functional structural element from a host mRNA, for its benefit (Taylor, 2020). A host selenoprotein mRNA's SECIS element could be captured by a viral mRNA via antisense

tethering and provide the necessary component to decode a viral UGA codon (Figure 4) (Taylor et al., 2016).

Figure 4. Proposed Mechanism of Viral mRNA Capturing the SECIS Element of a Host Selenoprotein mRNA



Note: Viral mRNA (green) is bound to the ribosome and is tethered downstream to a host selenoprotein mRNA (red) at the 3' untranslated region. The host mRNA contains the SECIS element, which can allow the viral mRNA to recode its UGA stop codon as Sec, adding it to the growing peptide chain instead of terminating translation.

EF = elongation factor; SBP2 = SECIS binding protein 2.

A virus may also capture a host mRNA to induce frameshifting, potentially using the ATI for a similar function as a pseudoknot by having complementarity to a sequence downstream of a slippery sequence heptamer (Henderson et al., 2006). These ATIs would be yet another example of viruses working against their constrained genomes to maintain their existence.

CHAPTER II: VALIDATED ANTISENSE TETHERING INTERACTIONS BETWEEN HOST SELENOPROTEIN AND VIRAL MRNAS

Introduction

Viruses use nucleotide interactions between their own mRNAs and ours in order to manipulate the expression of the host proteins as well as affect viral protein expression and genome replication (Skalsky & Cullen, 2010) (Lei et al., 2022) (Taylor, 2020). This relies on the complementarity of viral:host RNA:RNA sequences, and predicted interactions can potentially be found within a set of host and pathogen genomes. Several potential antisense interactions were found computationally between human mRNAs and viral mRNAs. Of these, several of the human targets were from selenoprotein mRNAs. Our group had previously used these methods to find antisense interactions between various viral mRNAs and human selenoproteins (Taylor et al., 2016) (Dailey et al., 2021). Given the relevance of selenoproteins to viral infection, the RNA:RNA interactions at play were a natural target of focus (Beck et al., 2004) (Guillin et al., 2019). Selenium deficiency increases virality, and likewise its supplementation mitigates the deleterious effects of infections, making selenoproteins a viable target for antisense tethering (Steinbrenner et al., 2015). Alongside human targets, the fruit bat, a speculated reservoir for SARS-CoV-2 was selected (Banerjee et al., 2019). These sequence alignments were found using BLAST (<http://blast.ncbi.nlm.nih.gov/Blast.cgi>) and then assessed using the RNAHybrid 2.2 (<http://bibiserv2.cebitec.uni-bielefeld.de/rnahybrid>) and the IntaRNA (<http://rna.informatik.uni-freiburg.de/IntaRNA/Input.jsp>) that analyze the interactions from the perspective of RNA:RNA interactions, which are more complex than simple complementarity (Rehmsmeier et al., 2004). These programs find the most stable and favorable region of interaction between the 2 submitted

sequences, allowing for some base pair mismatching and loops that can form in RNAs. With the IntaRNA program in particular, the strength of the interaction is calculated (kcal/mol) to show that the potential regions of complementarity will not only find each other in a solution of numerous other variable RNAs, but also overcome the energy needed to undo the internal base pairing of each single strand. Lower energies indicate a stability in the matches between separate strands over the sum of the individual intramolecular folding energies of each.

These predicted antisense interactions were then verified using gel shift assays to demonstrate the interactions in a physical space between DNA oligo models. If the sequences are truly complementary, then they will find each other in solution and maintain a duplex while moving through the gel. This duplex would be heavier due to being double the weight of the individual strands, meaning it would move slower through the gel, and appear further up when imaged.

Materials and Methods

Generation of Antisense Matches

Potential antisense interactions between host and virus RNAs were found using BLAST searches. Viral genomes were used as queries against human targets using the nucleotide-nucleotide function (blastn), starting with default parameters against the Reference RNA Sequence Database (refseq.rna), restricted to the target of Human RNA (*Homo sapiens* taxid: 9606) or other taxa. Various regions of complementarity were found between SARS-CoV-2 (NC_045512) and human TXNRD3 (NM_052883.2) and the 1976 strain of Ebola virus (MN416402.1) and human DIO2 (NC_000014.9). Complementarity was also found between SARS-CoV-2 (NC_045512) and fruit bat TXNRD3 (XM_006911434). Both the RNAHybrid

and IntaRNA programs were used to further assess the interactions between the results from BLAST. These results generated a “core” antisense region on each strand (Figures 5-7).

Gel Mobility Shift Assays

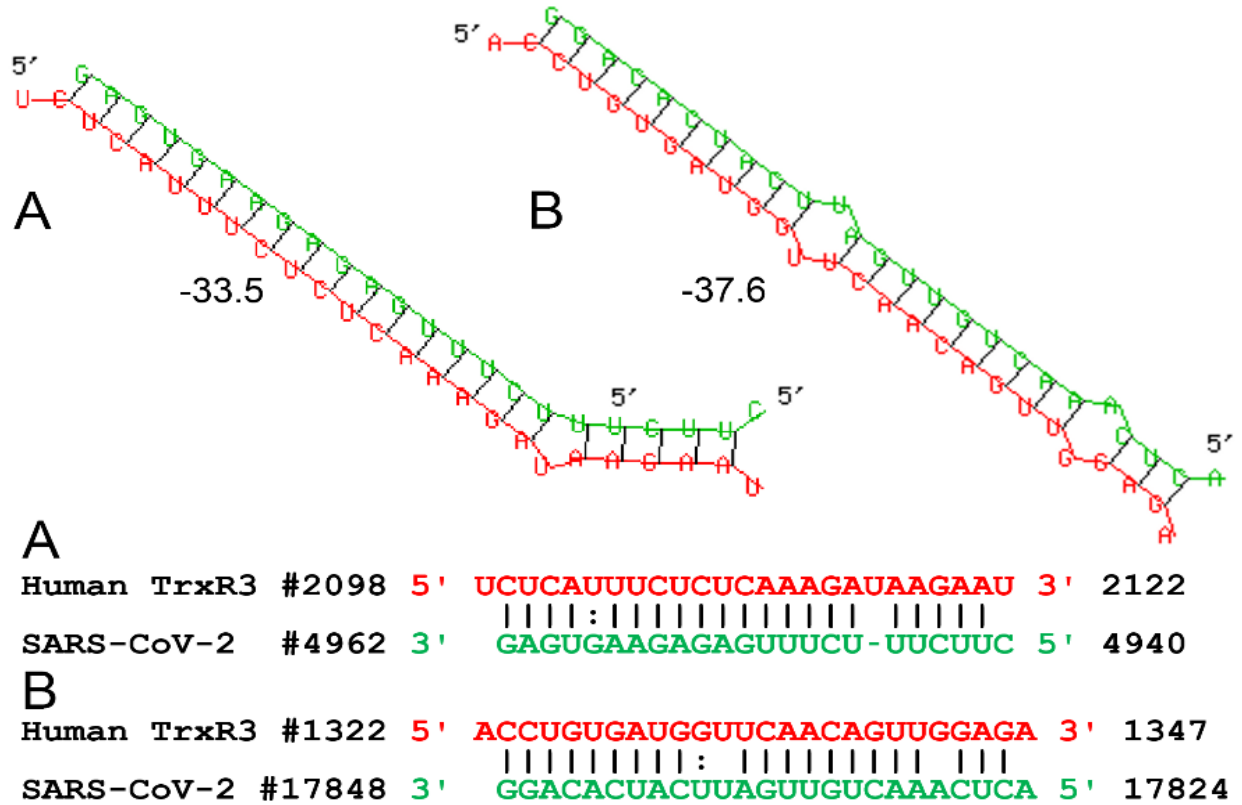
The oligos used in the gel shift assay were bases 17814–17858 of NC_045512 (coronavirus oligo C) and bases 1312–1357 of NM_052883.2 (TXNRD3 oligo T). A randomly shuffled version of viral sequence C was generated and labeled as R in Figure 4. Oligos were ordered from Integrated DNA Technologies, Inc., Coralville, IA.

The lyophilized DNA was dissolved in PBS to create 1 μ M stock solutions, which were stored at 4° C. One microliter of each sample (T, C, or R) was further diluted in PBS to a total volume of 10 μ L (at 100 nM). Oligos, either singly or in pairs of equal volumes of T + C or T + R, were incubated at room temperature for 1 hour. The tubes were then heated at 66° C for 15 minutes, and then cooled at room temperature for 40 minutes. Along with 2 μ L of loading dye, the DNA was placed into the lanes, using 10 μ L of either the single strands or pair mixtures, giving about 1 pmol of total DNA per well. The 5% TBE agarose gel, with ethidium bromide, was run at 65v for 4 hours while the setup was chilled in ice water. The gel was then analyzed and imaged with a BIO-RAD Gel Doc™ XR+ Molecular Imager.

Results

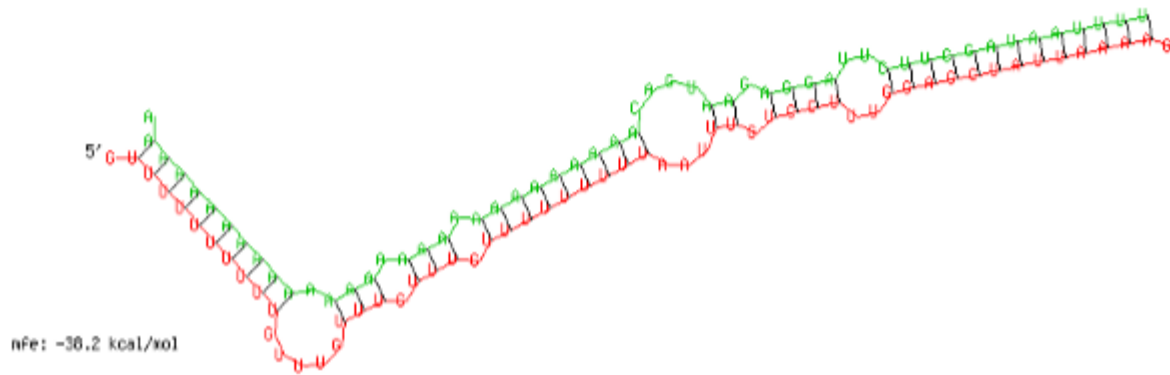
The computational and gel shift assay results for each of the predicted antisense interactions are presented below with details in the legends of Figures 5-10.

Figure 5. Predicted Antisense Interactions Between Human Thioredoxin Reductase 3 mRNA (Red) and SARS-CoV-2 mRNA (Green) Forming RNA Duplexes



Note: Interactions were first found using BLAST, then assessed further using RNAHybrid 2.2 and IntaRNA. Free energies in kcal/mol are shown next to each structure—presented as both secondary structures and as sequence alignments (Taylor, 2020).

Figure 6. Predicted Secondary Structure of an Antisense Interaction Between Fruit Bat Thioredoxin Reductase 3 mRNA (Red) and SARS-CoV-2 mRNA (Green) Forming an RNA Duplex



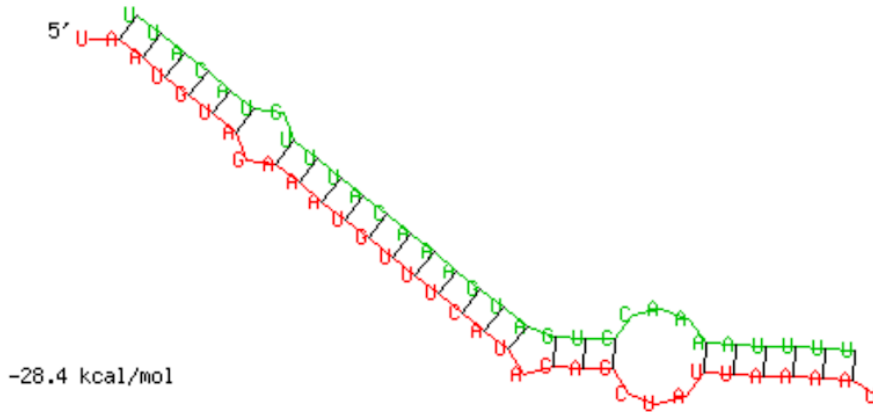
Note: Interactions were first found using BLAST, then assessed further using RNAHybrid 2.2 and IntaRNA. Free energies in kcal/mol are shown next to the structure.

Figure 7. Predicted Antisense Interaction Between Human Iodothyronine Deiodinase II mRNA (Red) and Zaire Ebola Virus Pol mRNA (Green) Forming an RNA Duplex

Ebola Pol vs. DIO2:

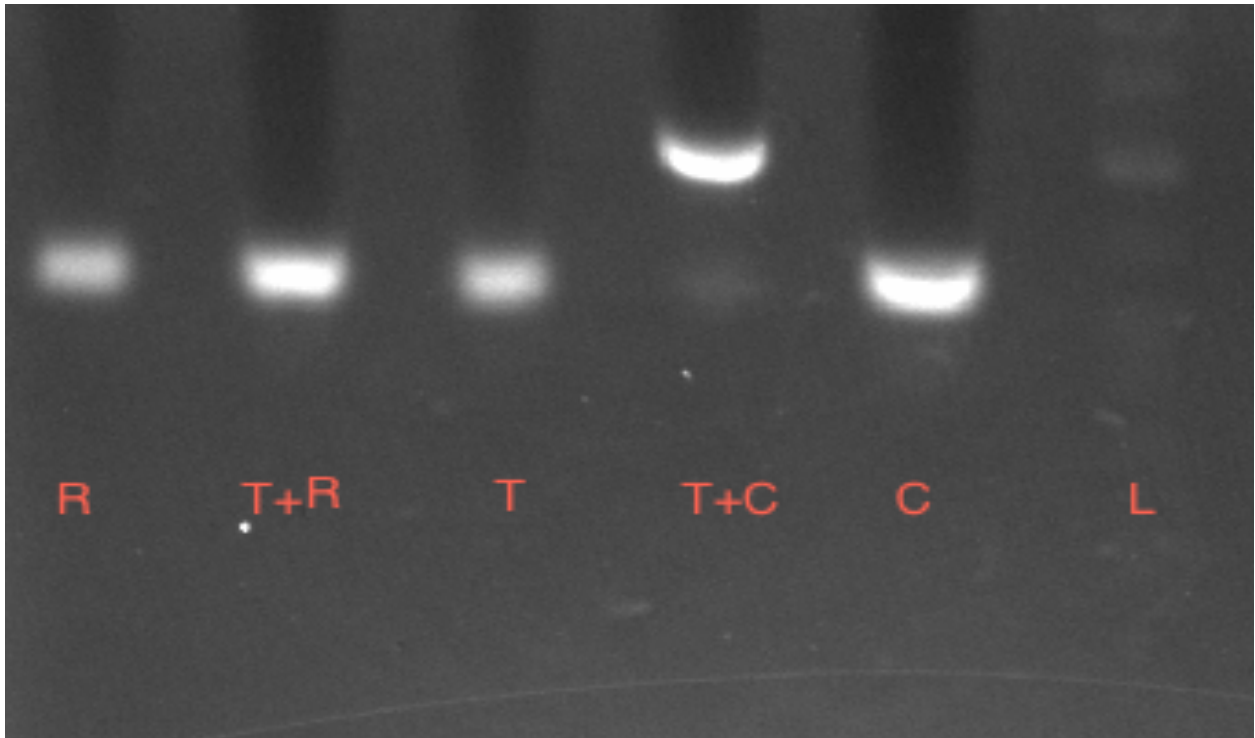
mde of **Ebola Pol**: -47.599998
TARGET : DIO2 length: 6148
MIRNA : **Ebola Pol** length: 30
mfe: -28.4 kcal/mol

position 4119
target 5' U G A CUA U 3'
AAUGUA AAAUGUUUCAU CAG UAAAA
UUACAU UUUACAAAGUA GUC AAUUUU
miRNA 3' G CAA 5'



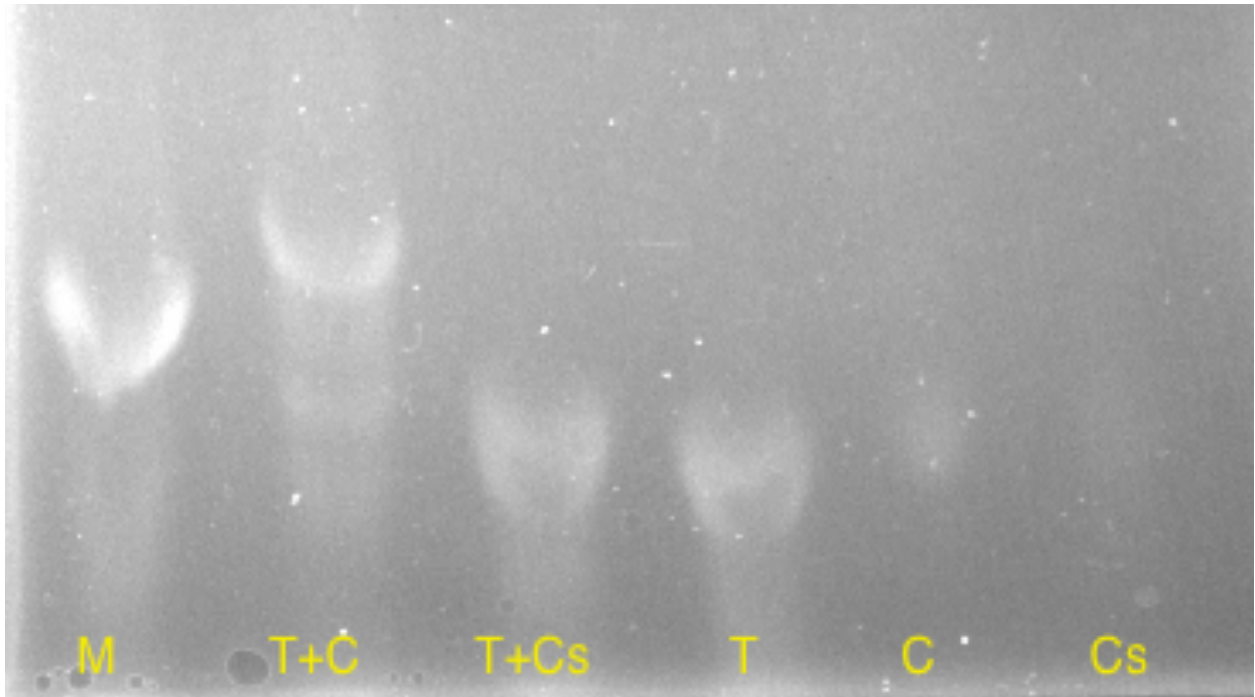
Note: Interactions were first found using BLAST, then assessed further using RNAHybrid 2.2 and IntaRNA. Free energies in kcal/mol are shown next to the structure—presented as both secondary structures and as sequence alignments.

Figure 8. Gel Mobility Shift Assay Validating the Antisense Tethering Interaction Between Human Thioredoxin Reductase 3 DNA and SARS-CoV-2 DNA



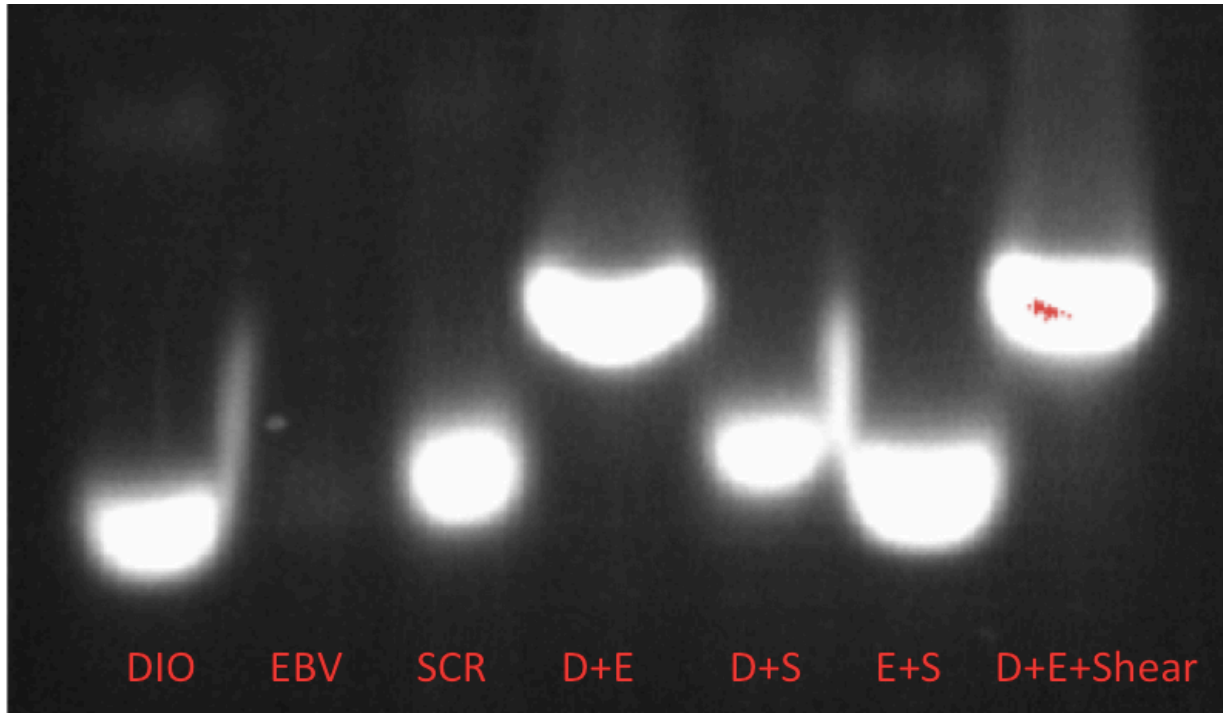
Note: Extended sequences from Figure 5 B were validated. The labels in each lane represent different single-stranded DNA oligonucleotides, where (T) is TNXRD3, (C) is SARS-CoV-2, (R) is a scramble of the SARS-CoV-2 sequence, and (L) is a molecular weight ladder. Paired lanes contain both corresponding oligos. All single sequence lanes and the T+R lane migrate as single strands, whereas the T+C lane migrates slower as a duplex. This indicates that the antisense interaction occurs between the T and C oligos as they are migrating as the sum of the 2 single strand weights instead of each individually moving in tandem, as you would see in the T+R lane. The duplex weight matches the predicted weight, as it is aligned with its corresponding ladder on the right side (L) (Wang et al., 2021).

Figure 9. Gel Mobility Shift Assay Validating the Antisense Tethering Interaction Between Fruit Bat Thioredoxin Reductase 3 DNA and SARS-CoV-2 DNA



Note: The labels in each lane represent different single-stranded DNA oligonucleotides, where (T) is fruit bat TNXRD3, (C) is SARS-CoV-2, (Cs) is a scramble of the SARS-CoV-2 sequence, and (M) is a marker chosen for the predicted weight of the T+C duplex. Paired lanes contain both corresponding oligos. All single sequence lanes and the T+Cs lane migrate as single strands, whereas the T+C lane migrates slower as a duplex. This indicates the antisense interaction occurs between the T and C oligos as they are migrating as the sum of the 2 single strand weights instead of each individually moving in tandem, as you would see in the T+Cs lane.

Figure 10. Gel Mobility Shift Assay Validating the Antisense Tethering Interaction Between Human Iodothyronine Deiodinase II DNA and the Ebola Polymerase (L) DNA



Note: The labels in each lane represent different single-stranded DNA oligonucleotides, where (DIO or D) is human deiodinase II, (EBV or E) is the Ebola L gene, (SCR) is a scramble of the DIO sequence, and the shear lane is herring sperm DNA, a complex of DNA used to represent the cellular environment of competing oligonucleotides. Paired lanes contained both corresponding oligos. All single sequence lanes and the E+S lane migrate as single strands, whereas the D+E lane migrates slower as a duplex. This indicates that the antisense interaction occurs between the DIO and EBV oligos, as they are migrating as the sum of the 2 single-strand weights instead of each individually moving in tandem, as you would see in the E+S lane. The 2 oligos in the shear lane are still able to tether despite the abundance of alternative DNA, indicating the interaction is most favored between the two.

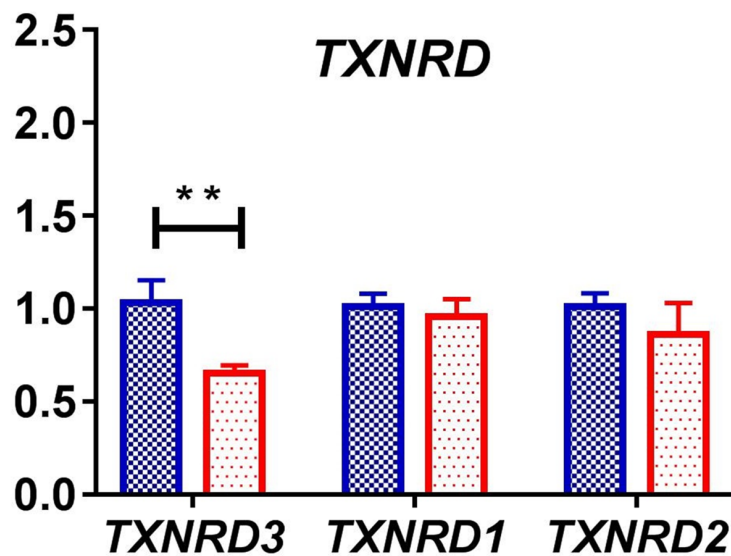
Discussion

Both TXNRD3 sequences and DIO2 were found to form the duplexes with the expected SARS-CoV-2 or Ebola-based oligos when run on a gel, as the paired oligos all migrated more slowly than the oligos run individually lanes. Notably, when one of the paired oligos was a scrambled sequence of the same composition as the paired strand, the two-migrated as a single strand, indicating there was no duplex formation, as the sequences were not complementary.

These interactions from Figures 8-10 are added to the growing list of viral:host RNA:RNA interactions, specifically in regards to selenoprotein mRNA. Yet, in the case of TXNRD3, only it was found to be computationally targeted for potential antisense interactions by SARS-CoV-2 amid its family of selenoproteins (Wang et al., 2021) (Taylor, 2020). TXNRD1 and 2 are expressed in a multitude of cell types, whereas TXNRD3 is mostly found expressed in the testes. Despite the ubiquity of the former to proteins across the body, TXNRD3 is involved with a function most vital to RNA viruses: DNA production. As TXNRD3 is part of the DNA synthesis pathway, in which ribonucleotides are a substrate, it is a potential target for knockdown to increase the amount of available ribonucleotides present in the cell (Holmgren & Sengupta, 2010). Ribonucleotide reductase uses thioredoxin as a hydrogen donor to convert ribonucleotides to the deoxyribonucleotide precursors. Without the reduced form of thioredoxin, this process cannot take place. SARS-CoV-2, being an RNA virus, would invariably benefit from an enhanced pool of ribonucleotides to replicate its genome, and anything that detracts from that would be a potential target. The knockdown of TXNRD3 mRNA (Figure 11), but not TXNRD1 or 2 (Wang et al., 2021), would work in tandem with the knockdown of TXNRD1 by the SARS-CoV-2 main protease, which was recently shown by Gallardo et al. (Gallardo, 2022). TXNRD2

is a mitochondrial isoform of the enzyme and may not have a significant effect on TRX redox balance outside of that organelle.

Figure 11. Relative mRNA Levels of Thioredoxin Reductase Isoforms in Uninfected Cells (Blue) and SARS-CoV-2 Infected Cells (Red), Measured via Real-Time Polymerase Chain Reaction



Note: Cells infected with SARS-CoV-2 show a decrease in the amount of TXNRD3 mRNA, while other isoforms maintain their relative cytoplasmic levels (Wang et al., 2021). It should be noted that mRNA levels do not correspond directly to protein level in every case (i.e., a 10% decrease in mRNA does not necessarily result in a 10% knockdown of the protein encoded by the mRNA). This is especially the case with selenoproteins given their complexity in expression and the levels at which they can be regulated.

This strategy could be applied to other mammalian systems, like the fruit bat, which are a natural reservoir for potential zoonotic transmission of pathogenic coronaviruses like SARS-CoV-2 and could explain the virus's development toward this particular method of virulence in humans. Viruses that successfully infect humans would have developed a system within

reservoir species to replicate efficiently within the hosts cells. Given the sequence homology between human and bat TR3, SARS-CoV-2 may have been well prepared to use the strategy of knockdown for human infections.

As for the case of DIO2 and Ebola L, that will be discussed in Chapter IV where the antisense interaction could serve a purpose outside of antisense-mediated knockdown.

CHAPTER III: SELENIUM-DEPENDENT READTHROUGH OF A 3'-UGA STOP CODON
IN THE NUCLEOPROTEIN GENE OF EBOLA VIRUS

Introduction

Previous work in our group analyzed the antisense interactions between several viral mRNAs and host selenoprotein mRNAs (Taylor et al., 2016). In the cases of the HIV *nef* gene and the Ebola nucleoprotein (NP) gene, both had regions antisense to isoforms of human TXNRD (Taylor et al., 2016). As with the coronavirus, all are RNA viruses that could potentially benefit from the knockdown of TXNRD by decreasing the synthesis of deoxyribonucleotides and thus increasing the available pool of ribonucleotides, as discussed in Chapter II. There exists the possibility of additional benefits to this interaction, however. In both, the *nef* and NP terminate in a conserved UGA stop codon that could potentially be recoded as SeC. Previous work by Dr. Taylor had focused on HIV-1 to show that the virus can encode a functional selenoprotein, GPx, in an overlapping reading frame of the gp120 viral envelope protein (Zhao et al., 2000). Despite showing activity, the construct used to express the GPx had to include an exogenous mammalian SECIS element as well as a serine residue in place of a cysteine to achieve this functionality. No functional SECIS element was found in the sequence, but the possibility exists that a tethered host selenoprotein mRNA could serve to provide that needed SECIS element for the virus.

In the case of the NP gene, it is necessary to show that the UGA codon would serve to encode a SeC in the first place. Our group has performed some work to show that there is selenium-dependent readthrough of that 3' UGA stop codon (E. W. Taylor et al., 2015). The initial experiment of demonstrating stop codon readthrough, as well as selenium-dependent readthrough, will be replicated. Further experiments will be conducted to validate the presence of

a selenium within the readthrough product, as well as validate the effect of antisense tethering as a way to capture a host's SECIS element.

The initial experiment involves a construct designed to assess the readthrough component of the NP. An in-frame green fluorescent protein (GFP), downstream of the 3' UGA stop codon, will only be expressed if readthrough occurs. If readthrough does not occur, then no GFP will be expressed. With the addition of sodium selenite, the readthrough could be enhanced by increasing the available concentration of SeC, which is at a much lower concentration in the cell than other amino acids (Turanov et al., 2015). Increasing the amount of cellular SeC via sodium selenite could increase the rate at which readthrough occurs. The effect on the readthrough construct would be an increase in GFP signal compared to cells treated with the construct but no additional sodium selenite. A dose-response curve will be generated to determine the potential range of sodium selenite concentration needed for a significant increase in readthrough.

Materials and Methods

Cell Culture

Growth media was prepared using 220 mL of 1x DMEM media (Gibco™ catalog number 11054020), 25 mL heat-inactivated FBS (Gibco™ catalog number 10082147), 2.5 mL 100X L-glutamate (Invitrogen catalog number 25030081), and 2.5 mL Penicillin-Streptomycin (Gibco™ catalog number 15070063). All components were sterilized through a 0.22-micron vacuum filter. For the initial seeding, HEK293T cells were obtained from liquid nitrogen storage and thawed at 37° C. The cells were then centrifuged for 1 minute, with the supernatant being discarded before the cells were resuspended in 1 mL of fresh warm media. The 1 mL of cells and 4 mL of media were added to a T-25 flask and incubated for 3 days at 37° C and 5% CO₂. Cells had their media changed and were washed with 1X phosphate buffer saline.

When cells were at 90% confluency, they were exposed to 2 mL of 1 mL of TrypLE™ Express Enzyme (1X, no phenol red, Gibco™ catalog number 12-604-013) for 10 minutes. The cells were then spun at room temperature for 3 minutes. The supernatant was removed, and the cells were resuspended with 975 µL of fresh media. A total of 20 µL of these cells were added to 20 µL of 0.4% Trypan blue solution (Gibco™ catalog number 15250061). A total of 10 µL of this solution was added to a Countess™ II (Invitrogen™ catalog number AMQAX1000) to determine cell viability and number. The approximate 1-mL cell suspension was then added to a new T25 or a T75 dependent on cell number.

For cell storage: 1 million cells were added to 900 µL of fresh media, 100 µL of dimethyl sulfoxide, and stored at -4° C at 1 hour, then at -80° C for 24 hours, then stored in liquid nitrogen.

Engineering of GFP Expression Vectors Designed to Validate UGA Stop Codon

Readthrough

To assess the potential readthrough of the 3' UGA codon in the Ebola NP gene, a fragment of the gene (J04337.1, 2212-2689) was inserted into a pUCIDT-Kanamycin plasmid from IDT (Integrated DNA Technologies, Inc, Coralville, IA) using a 5' BglII and a 3' HindIII restriction site on the corresponding ends. The insert was placed into the multiple cloning site upstream of a GFP gene, which would be past the 3'UGA of the NP fragment in the same frame (Figure 13).

Plasmid Propagation

Full constructs were propagated using JM109 bacterial cells and purified using a PureYield™ Plasmid Miniprep system by Promega (Catalog number A1222). A total of 50 µL JM109s were thawed on ice for 30 minutes then mixed with 1 µL of plasmid DNA at 250 ng/µL

for an additional 30 minutes. Cells were then heat shocked by placing them at 42° C for 45 seconds then on ice again for 2 minutes. The bacteria were then added to 1 mL of SOC (Super Optimal broth with Catabolite repression) media and incubated at 37° C for 45 minutes while shaken. The outgrowth solution was then added onto an LB agar plate by T-stroking and incubated for 24 hours at 37° C. Isolated colonies were picked and grown in Luria Broth with 100 ug/mL kanamycin overnight. Plasmid isolation/purification was performed using a Promega PureYield™ Plasmid Midiprep System (Promega, A2492) kit, per manufacturer's protocol, except the final plasmid elution was with 30 µL of 80° C nuclease-free water. Plasmid concentrations were measured with DeNovix DS-11 spectrophotometer and stored at -4° C.

Transfer of Viral Inserts to pAcGFP-N1 Plasmid

Initial plasmids underwent a double digestion with BglIII and HindIII overnight. Digestion products were run on a 2% (approximately) TAE gel at 65V for 2 hours and verified using a BIO-RAD Gel Doc™ XR+ Molecular Imager. Bands were excised and purified using a WizardTMSV Gel and PCR Clean-up System (Promega, A9281), following the manufacturers recommended protocol. Purified inserts were ligated into new pAcGFP-N1 plasmids using a T7 DNA ligase during an overnight incubation. These new products were transformed into new JM109s, and the propagation protocol was repeated. Proper plasmid sequences were verified by sequencing at (Eurofins Genomics, Louisville, KY). Once verified, transformants from the previous step were used to inoculate a 330 mL LB broth culture. A PureYield™ Plasmid Midiprep System (Promega, A2492) was performed to gather the final set of new plasmid.

Transfection Protocol

Cells were seeded in 24 well plates with 100,000 cells per well, with 500 µL of media and incubated for 24 hours at 37° C at 5% CO₂. A total of 50 µL of Opti-MEM I (Gibco catalog

number 31985070) was incubated with 1 ug of plasmid DNA; 3 μ L of 1 mg/mL polyethylimine (PEI) was incubated with 50 μ L of Opti-MEM for 5 minutes at room temperature. Both solutions were then mixed and incubated for 20 minutes at room temperature. The lipid-DNA complexes were then added to the appropriate wells, and the cells were then incubated again for 48 hours.

Reporter Gene Assays

After transfection and incubation, Fluorescence was measured from the cells directly first using a Flexstation II multimode plate reader (Molecular Devices, San Jose, CA). The following settings were used:

Fluorescence

Bottom Read

Wavelengths: Ex. 485 nm, Em. 538 nm, auto cut-off 530 nm

Sensitivity: Readings: 6, PMT: Auto

Automix: Before: Off

Autocalibrate: On

Assay Plate Type: Costar Clr 24 Well PLate

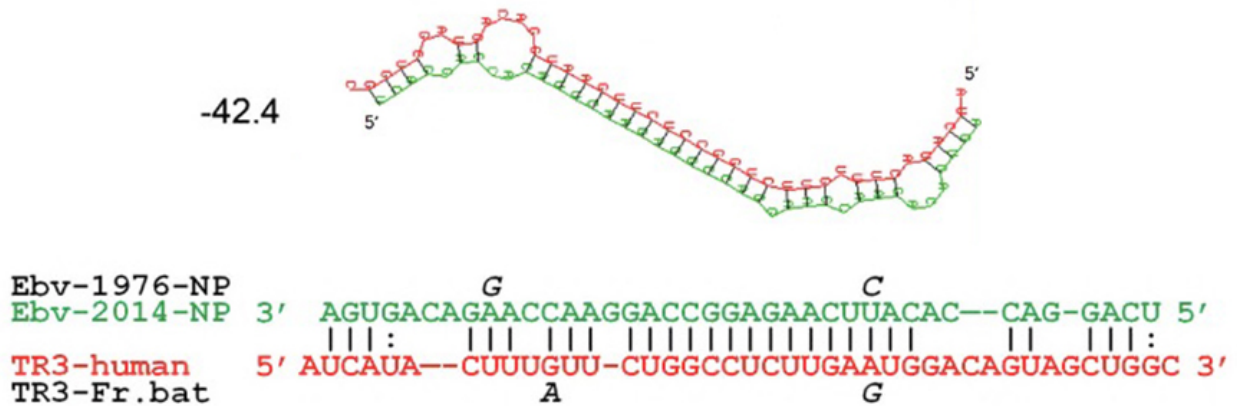
Wells to Read: (selected wells only)

Column Wavelength Priority: Column Priority

Auto read: Off

Results

Figure 12. Predicted Antisense Interactions Between Human Thioredoxin Reductase 3 mRNA (Red) and Ebola Nucleoprotein mRNA (Green) Forming RNA Duplexes



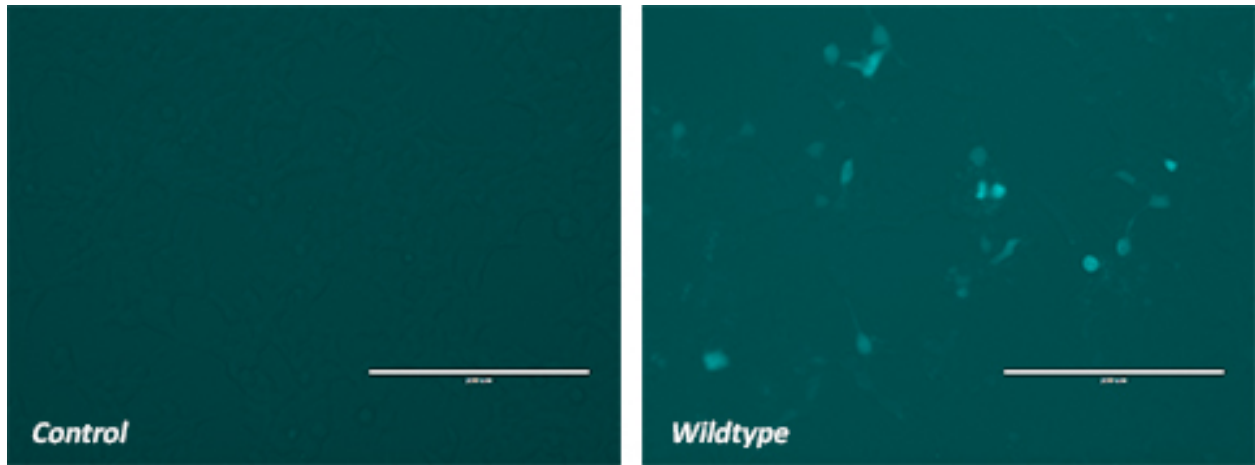
Note: Interactions were first found using BLAST then further assessed using RNAHybrid 2.2 and IntaRNA. Free energies in kcal/mol are shown next to the structure—presented as both secondary structures and as sequence alignments. Sequence differences between the 1976 Ebola strain (AF086833.2) are above the 2014 sequence (KP271020.1) (green). The sequence differences for fruit bat and human TR3 are also displayed below (red).

Figure 13. General Design of the Ebola Nucleoprotein Gene Readthrough Construct



Note: The Ebola NP gene is inserted in the same frame prior to a GFP gene. If readthrough occurs, translation will not stop at the NP gene's 3' UGA and continue to translate the GFP gene downstream.

Figure 14. Terminal 3' UGA Codon in the Ebola Nucleoprotein Is Recoded as Selenocysteine in HEK Cells



Note: Cells transfected with the Ebola NP readthrough construct (right) containing 3' UGA codon prior to a GFP reporter gene, only have GFP is expressed in the wildtype when readthrough occurs. The negative control (left) shows the basal level of fluorescence of HEK cells under a fluorescent microscope.

Table 1. Fluorescent Reads of HEK Cells Transfected With Nucleoprotein Readthrough Construct

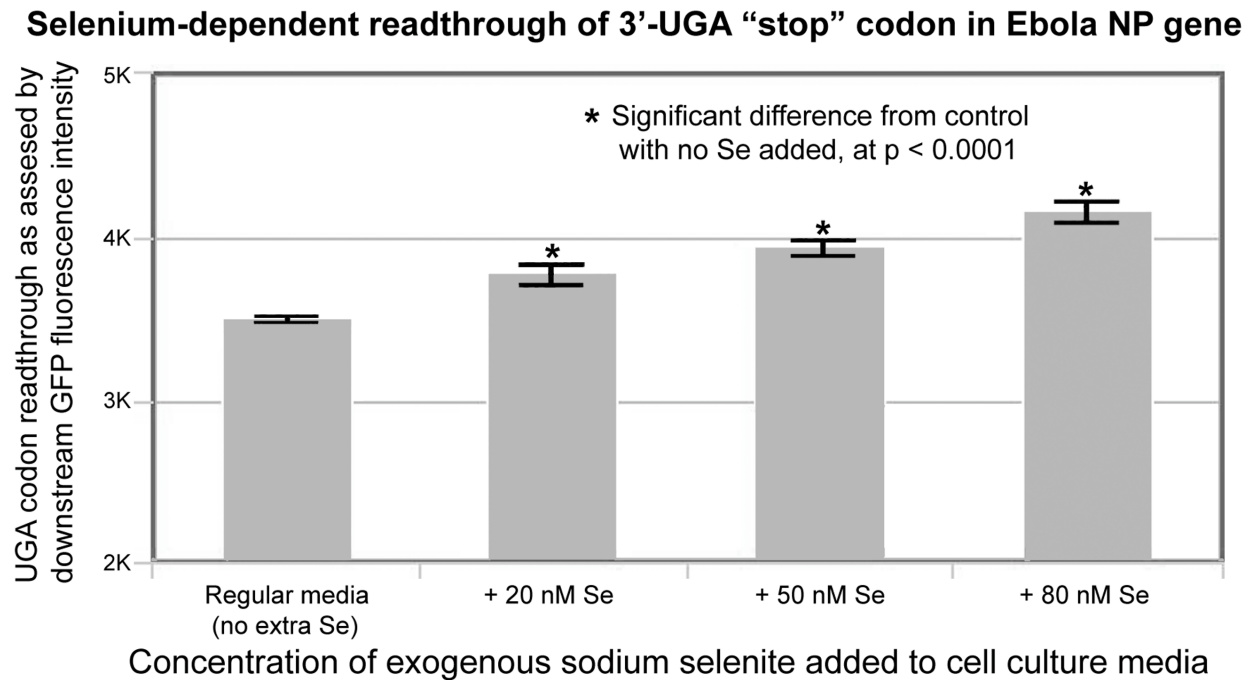
Ebola NP	Control	Wildtype
1	21998	26764
2	24335	26922

Ebola NP	Control	Wildtype
3	20192	25372
4	22136	25365
average	22165.25	26105.75
SEM	848.054575	426.873981

Note: A single experiment was carried out to demonstrate the readthrough component of the Ebola NP gene.

NP = nucleoprotein; SEM = standard error of the mean.

Figure 15. Selenium-Dependent Readthrough of UGA Stop Codon in Ebola Nucleoprotein Gene



Note: Sodium selenite added to media at the time of transfection at 20 nM, 50 nM, and 80 nM results in an increase in readthrough. When more selenium is available, the rate of successful readthrough increases as there are now more accessible SeC tRNAs to be incorporated into the peptide. This is preliminary unpublished data obtained from our group.

Discussion

GFP levels in the wildtype readthrough construct, containing the NP gene and its 3' UGA stop codon, were shown to increase significantly compared to cells without the construct (Figure 14). Any presence of GFP in the readthrough cells (image 3 of Figure 14) indicates readthrough has occurred by some mechanism. The untransfected HEKs have naturally low levels of fluorescence, and the fluorescent signal from the readthrough construct comes from the in-frame GFP that is past the NP gene. Since the NP gene still contains its 3' UGA stop codon, the recoding of that UGA to SeC could potentially explain why readthrough occurs. While the potential for readthrough suppression via suppressor tRNAs exists, future experiments will contain a full negative control featuring 3 stop codons in tandem prior to the GFP. While the possibility exists that the stop codon is recoded as SeC, demonstrating readthrough alone does not prove this to be the case. The SECIS element that could be provided to the NP gene via an ATI will be demonstrated using a future construct containing a scramble of the antisense region of the NP gene prior to the UGA stop codon. If the SECIS element is brought with the TR3 mRNA with antisense tethering, then a scramble sequence with no complementarity would not be tethered to the host mRNA containing the SECIS element. This would prevent the recoding of UGA as SeC and prevent the downstream GFP from being translated. This ATI scramble construct would have similar GFP levels to the negative control, as neither would have significant levels of readthrough.

There is a case for the involvement of a SECIS element, as readthrough appears to have been dependent on selenium levels in the cell (Figure 15). Wells containing cells exposed to increasing concentrations of sodium selenite showed a significant increase in readthrough via GFP expression, at $P < 0.0001$, when compared to the control group. The control group featured the readthrough construct, but no additional selenium beyond the basal concentrations in the applied media, indicating the readthrough that does occur with this construct is enhanced by the addition of selenium. As stated before, the rate of stop codon readthrough can be dependent on the amount of available selenocysteinyl-tRNAs. This is the case for a particular codon; the longer it takes for the ribosome to receive a particular aminoacyl-tRNA, the greater the chance it has of termination.

CHAPTER IV: A NOVEL RIBOSOMAL FRAMESHIFT SITE IN THE POLYMERASE

GENE OF EBOLA VIRUS

Introduction

With the analysis of sequences between viral and host mRNAs, several of which have been validated, there exists the possibility for further use of the captured elements for the virus. Initially, the ATIs were thought to be purely for knockdown, suppressing the expression of host proteins by interference with the translation of the mRNAs. While this is most certainly a potential benefit (Wang et al., 2021), Chapter III explored the possibility of a virus using the tethered host mRNA secondary structure (SECIS) during translation of the viral mRNA on the ribosome. In this chapter, we will examine a case of -1 ribosomal frameshifting in the Ebola virus polymerase (L) gene, which is unusual because an antisense interaction with the mRNA of the DIO2 selenoprotein maps onto the same location.

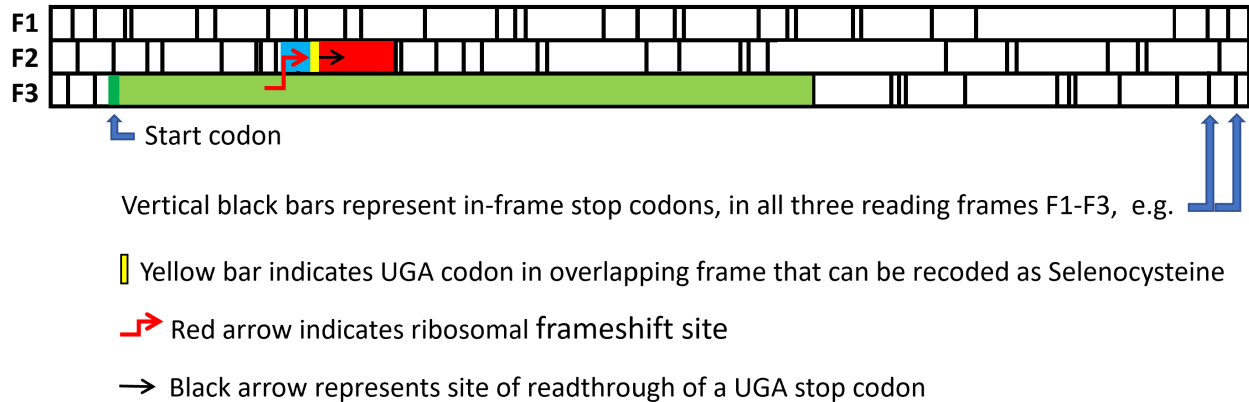
The predicted frameshift site in the Ebola L gene includes an RNA pseudoknot, which serves to create a pause at the ribosome upon reaching a particular sequence on the bound mRNA, the site of frameshifting at the slippery sequence heptamer. This intramolecular formation arises from internal complementarity, several bases from the slippery sequence, and is involved in the enhancement of frameshifting. Using the KnotinFrame program (Theis et al., 2008), Dr. Taylor was able to identify a possible frameshift site in the L gene of Ebola that could form a pseudoknot downstream of a slippery sequence heptamer (Figure 19). The program looks for that signature X XXY YYZ motif and then searches for regions of internal complementarity that can form pseudoknots shortly downstream. Our group's previous work has found frameshift sites in other RNA viruses that not only have functional frameshifts but also encode a functional

selenoprotein in an overlapping reading frame (Zhao et al., 2006). This has prompted analysis of other viral genomes, especially in ones without known frameshift sites.




A potential frameshift site was found to be within the Ebola polymerase gene, featuring an ideal slippery sequence of only A and T bases, preceding a sequence that could allow the formation of a pseudoknot (Figure 18). This same sequence of the L gene is found within same fragment that was identified as antisense to a host mRNA (Figure 7). This host mRNA happened to be a selenoprotein, and as we have discussed before, viral ATIs to human selenoproteins can potentially involve the capturing of host SECIS elements to recode UGA codons as SeC. This sequence does in fact contain a UGA codon, and not just one, but 2 geminal UGA codons in the minus 1 frame. The antisense interaction here could serve both to provide the SECIS element needed to recode the UGA codons and to form the necessary secondary structure to stall the ribosome to enhance frameshifting.

As shown in Figure 16, the product of this frameshift can result in truncated version of the fragment. Even if the UGA codons are translated as SeC, a new stop codon is reached soon after.

Figure 16. Schematic of a Hypothetical Gene With a -1-Frameshift Site Leading to an Overlapping Gene Variant With an In-Frame UGA Codon That May Be Recoded as Selenocysteine



Possible protein products depending on sequence of events:

-  Conventional protein product
-  Frameshift product terminated at UGA codon, acting as STOP
-  Frameshift followed by UGA stop codon readthrough (→)

Note: Two potential variant products exist from this frameshift: 1) A truncated version of the gene as a result of terminating at the -1 frame UGA codon; 2) A new modified version of the gene with an unknown function resulting from the recoding of the UGA as SeC. A similar gene topology is seen in the Ebola L gene, except there are 2 geminal UGA codons in the overlapping -1 reading frame.

Determining the function of this new product and assessing whether it contains a SeC is beyond the scope of the current project.

To assess the viability of antisense-mediated frameshifting, it was necessary to show that the predicted frameshift site was functional in the first place. A dual reporter construct was made to generate a ratio of 2 reporter gene signals to compare a wildtype frameshift sequence to a

frameshift knockout mutant. The design was such that the downstream signal, GFP, was in frame of the viral insert. If frameshifting occurs, then in that event the new reading frame would not contain a functional GFP protein and thus not generate fluorescence. The upstream signal, luciferase, would be used to confirm successful transfection of the plasmid into the cell. If no luciferase is present, then the construct as a whole is not being expressed inside the cell. This allows for variable amounts of cells to be in each well while still being able to accurately assess the presence of a frameshift. The mutant is designed to prevent frameshifting completely by altering the slippery sequence needed for a frameshift to occur, without modification of the translated protein. GFP would be expressed every time luciferase is expressed in this mutant construct. The wildtype will then be compared to the mutant, and a decrease the ratio of GFP to luciferase (G/L) would indicate a frameshift.

To evaluate the effect of ATIs on frameshifting after the frameshift site was found to be functional, the construct was then incubated with oligonucleotides corresponding to the antisense matches found between the L gene fragment and the DIO2 gene. These DIO2 oligos were used in the gel shift assays in Figure 10 and were already shown in Chapter II to be complementary to the L gene insert that was in the construct. If the tethering of the host mRNA enhances frameshifting, then there will be a decrease in the ratio of GFP to luciferase.

Materials and Methods

Frameshift Construct Design

The viral inserts for the frameshift construct were as follows:

Wild Type:

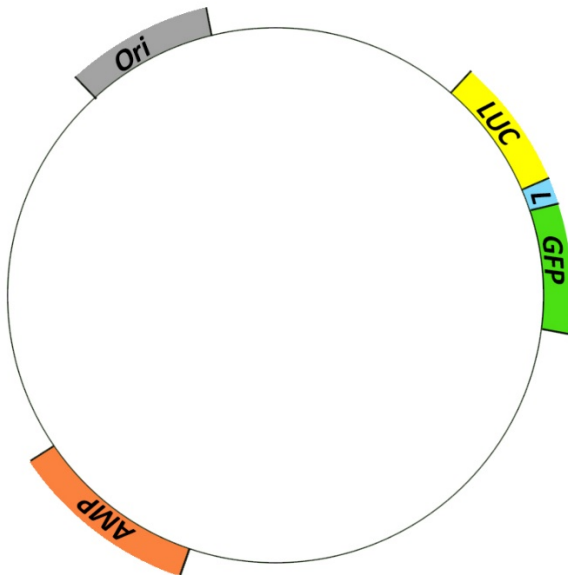
5' GGGACCC TTTAAAA CCTGATGAAATTTGTACATTCAGGTTTTATCTATTTGGAAA
AAAACAATATTTGAAT GAATTC 3'

Frameshift knockout Control (Mutant):

5'GGGACCCCTTGAAACCTGATGAAATTTGTACATTTAGGTTTTATCTATTTTGGAAA
AAAACAATATTTGAATGAATTC 3'

The insert features the sequence (13938-13989, MN416402.1) from Figure 18, extending 2 bases past the B' stem A, to an additional AT in each. This is to allow some space between the restriction site and the potential pseudoknot formation. An ApaI restriction site was added (in blue) to the 5' end, and an EcoRI (purple) restriction site was inserted to the 3' end. Underlined (in yellow) is the slippery sequence heptamer, TTTAAAA, in the wildtype insert. The mutant contains the same number of bases in that slippery sequence but with 2 point mutations. In order to knockout frameshifting, the slippery sequence needed to be altered in such a way as to prevent a new codon-anticodon pair but maintain the amino acid sequence that the wildtype had. The first T and first A of the slippery sequence was changed to a C and a G respectively. This removes the X XXY YYZ motif completely but allows each protein to keep a leucine (coded for by both TTA and TTG). The preceding codon of CCT in the wildtype that codes for proline still codes for that amino acid in the mutant with a CCC codon. Added upstream of this viral fragment was a luciferase reporter gene and downstream of the fragment was a GFP reporter gene, all in the same ORF. These full inserts were then ligated into a CMV plasmid containing a T7 promoter and an ampicillin-resistance gene. The general design appears as a circular plasmid (Figure 17) when fully inserted. The viral inserts were ordered from IDT (Integrated DNA Technologies, Inc, Coralville, IA).

Figure 17. General Schematic of the Dual Reporter Frameshift Construct



Note: At the multiple cloning site is a luciferase reporter gene (yellow), upstream of the viral insert containing the potential frameshift site (blue); downstream of the viral insert is the green fluorescent protein reporter gene (green).

Plasmid Propagation

Full constructs of both wildtype and mutant were propagated using JM109 bacterial cells and purified using a PureYield™ Plasmid Miniprep system by Promega (Catalog number A1222). A total of 50 μL JM109s were thawed on ice for 30 minutes then mixed with 1 μL of plasmid DNA at 250 $\text{ng}/\mu\text{L}$ for an additional 30 minutes. Cells were then heat shocked by placing them at 42° C for 45 seconds then on ice again for 2 minutes. The bacteria were then added to 1 mL of SOC (Super Optimal broth with Catabolite repression) media and incubated at 37° C for 45 minutes while shaken. The outgrowth solution was then added onto an LB agar plate by T-stroking and incubated for 24 hours at 37° C. Isolated colonies were picked and grown in Luria Broth with 50 $\mu\text{g}/\text{mL}$ ampicillin overnight. Promega's manufacture protocol was

performed, eluting with 30 μ L of heated nuclease-free water. Plasmid concentrations were measured with DeNovix DS-11 spectrophotometer and stored at -4° C.

Transfection Protocol

Cells were seeded in 24 well plates with 100,000 cells per well, with 500 μ L of media and incubated for 24 hours at 37° C at 5% CO_2 . A total of 50 μ L of Opti-MEM I (Gibco catalog number 31985070) was incubated with 1 μ g of plasmid DNA; 3 μ L of 1 mg/mL PEI was incubated with 50 μ L of Opti-MEM for 5 minutes at room temperature. Both solutions were then mixed and incubated for 20 minutes at room temperature. The lipid-DNA complexes were then added to the appropriate wells, and the cells were then incubated again for 48 hours.

Reporter Gene Assays

After transfection and incubation, cells were lysed with 200 μ L Reporter Lysis Buffer (Promega, catalog number E4030). A total of 100 μ L of the lysate was added to each well of a Costar 96 clear bottom black well plate. Fluorescence was measured first using a Flexstation II multimode plate reader (Molecular Devices, San Jose, CA). The following settings were used:

Fluorescence

Bottom Read

Wavelengths: Ex. 485 nm, Em. 538 nm, auto cut-off 530 nm

Sensitivity: Readings: 6, PMT: Auto

Automix: Before: Off

Autocalibrate: On

Assay Plate Type: 96 Well Costar blk/clrbtm

Wells to Read: (selected wells only)

Column Wavelength Priority: Column Priority

Autoread: Off

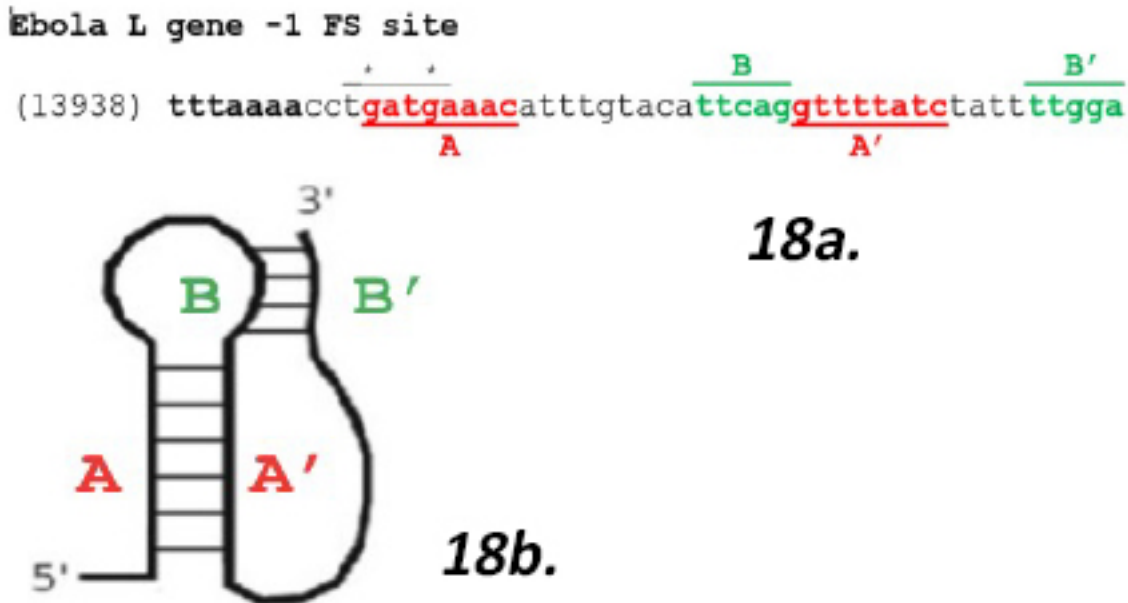
After the GFP was read, luminescence was read with the plate reader after using reagents from a ONE-Glo™ Luciferase Assay System (Promega, catalog number E6110) prepared using manufacturer's instructions. A total of 20 μL of 1X substrate was added to each well and incubated at room temperature for 10 minutes. After luminescence was selected, the settings were the same as fluorescence.

Antisense Induction of Ribosomal Frameshifting in Dual Report Assay Construct

MyTXTL T7 Expression Kit (Arbor Sciences, Ann Arbor MI, catalog number 505024) was used with the wildtype construct, with the addition of the DIO2 oligos used previously. The myTXTL LS70 Master Mix, the helper plasmid P70a-T7rnap and the positive control plasmid T7p14-deGFP were thawed on ice, along with aliquots of the plasmid and oligos. All tubes were vortexed and briefly centrifuged after thawing. Each reaction tube (GFP positive control, DIO2+, DIO2-, and a negative control) contained 9 μL LS70 Master Mix, 2.5 μL of plasmid DNA (333 nM) or the control (T7p14-deGFP at 24 nM), 0.5 μL of P70a-T7rnap (at 2.4 nM). The negative control had 2.5 μL of nuclease-free water in lieu of plasmid. A total of 0.75 μL of 100 nM DIO2 oligo was added to the DIO2+ tubes. All other tubes had an additional 0.75 μL of nuclease-free water added for a final volume of 12.75 μL . All tubes were incubated for 20 hours at 29° C. Reactions were stopped by placing the tubes on ice after incubation. The reaction solutions were then added to each well of a Costar 96 clear well black bottom plate and reads for fluorescence and luminescence were taken using the protocol from above. Only 10 μL of luciferase assay substrate were used in each well instead.

Results

Figure 18. Predicted Frameshift Site in the L Gene of Ebola Virus



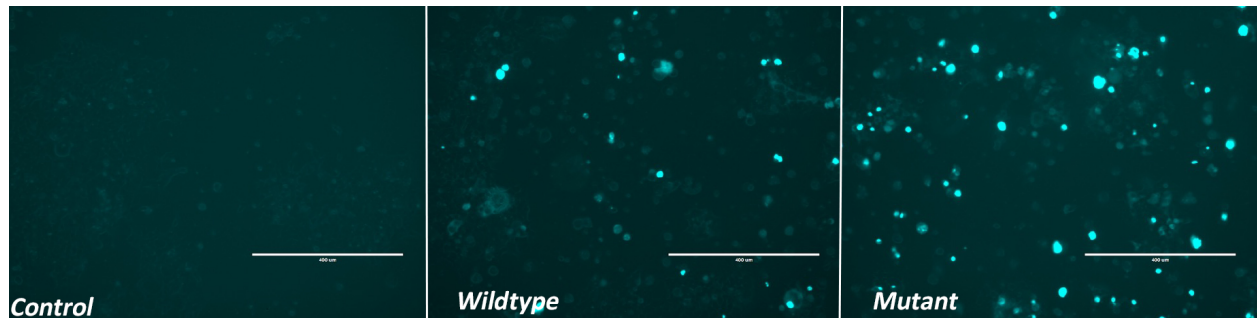
Note: The slippery sequence heptamer (TTTAAAA) in bold contains the X XXY YYZ motif that is observed in many -1 frameshift sites. Downstream after a few bases is a region that can form a pseudoknot. The first stem is formed by the pairing of sequence A and A' (in red) and the second stem is formed from the B and B' sequences (green). These can form the secondary structure in 16.

Figure 19. Predicted Ribosomal Frameshift Site in the L Gene of Ebola Virus Using the KnotinFrame Program

```
>Ebola L gene fragment
Rank: 1
Slippery sequence: tttaaaa
Slippery position: 338
Substring length: 60
Deltarel: 0.052
345 cctgatgaaacatttgtacattcaggtttatctatcttttggaaaaaacaatatttgaat 405
-9.60 ...[[[[[[[[[.....{{{[[]]]]]]]].....(((.....)))]]]]. knotted structure
```

Note: The predicted ribosomal frameshift site was found using the KnotinFrame program (Theis et al., 2008) using the Zaire Ebola virus L gene fragment (13601-14200, MN416402.1). The program identifies a slippery sequence heptamer with the motif X XXY YYZ in the 0 frame and then looks downstream for the potential for pseudoknot formation.

Figure 20. HEK293T Cells Taken From an EVOS Fluorescent Microscope 2 Days After Transfection



Note: Control cells were grown in media with no transfection reagents. The mutant and wildtype cells were transfected with their respective plasmids and express GFP relative to the amount of plasmid they contain. The control demonstrates the basal amount of fluorescence that the cells produce and can be used to validate successful transfection in the treatment groups. GFP levels of the mutant and wildtype are expected to be significantly higher than the control.

Table 2. Average Data From 7 Independent Experiments (A-G) Involving the Transfection of the Dual Reporter Frameshift Construct

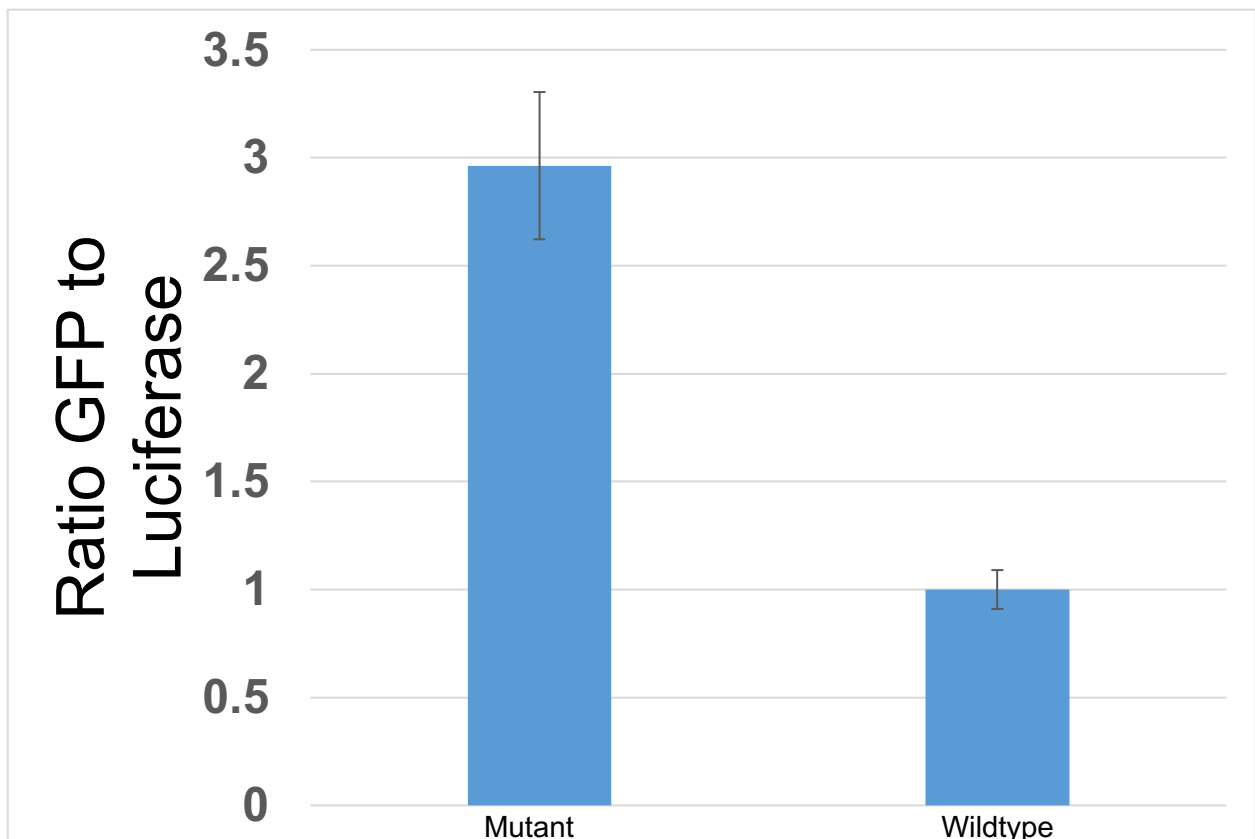
Expt.	G/L, mutant	Wild	G/L,	SD (s)	n
A	3.022	1	1	1.127	5
B	3.467	1	1	0.3836	5
C	2.623	1	1	0.5039	5
D	4.238	1	1	0.2671	4
E	2.967	1	1	0.3639	3
F	3.154	1	1	0.2349	6
G	1.273	1	1	0.1838	3

	G/L	SD (s)	SEM
Wildtype	1	0.5	0.09
Mutant	2.963429	0.902895	0.341

Note: The results in measured in GFP over luciferase signals. The data from Appendix tables A-G data were normalized to WT = 1. Below the table is the of all experimental averages, with calculated standard error of the means (SEMs). The results of the unpaired T-test at N = 7 was $P < 0.0001$ indicating a statistically significant difference between the wildtype and mutant groups.

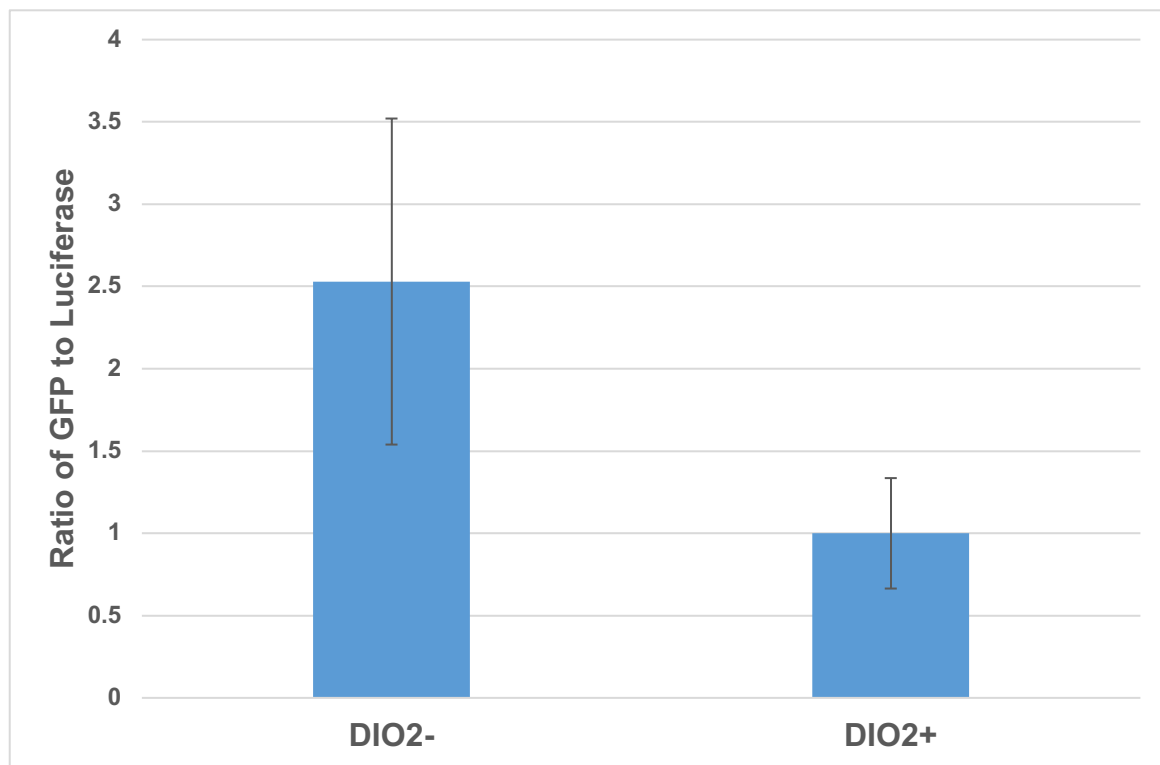
SD = standard deviation; SEM = standard error of the mean.

Figure 21. Ratio of Green Fluorescent Protein to Luciferase Signals of Dual Reporter Assay Construct for the Validation of a Functional Frameshift Site



Note: Data are expressed as the mean of 7 experiments (Appendix tables A-G, N = 7) \pm the SEM. Each ratio from each separate experiment was normalized to W = 1 in each experiment. The unpaired T-test results of $P < 0.0001$ suggest a significant difference between the 2 groups.

Figure 22. Ratio of Green Fluorescent Protein to Luciferase Signals of Dual Reporter Assay Construct After the Addition of Complementary Paired Sequences



Note: This was a single experiment done using the myTXTL kit, an in vitro translation system that allowed the simple addition of DIO2 DNA oligos to the reaction solution containing the frameshift construct with the L gene antisense sequence (DIO2+). A negative control group featured only the construct used previously and no addition of DIO2 (DIO2-). The ratio of GFP to luciferase was used to determine the level of frameshifting, and a decrease in the ratio would

indicate an increase in the event. The addition of DIO2 oligos appears to have some effect on the rate of frameshifting.

Discussion

The predicted frameshift site in the L gene of Ebola virus from Figure 18 has been shown to be functional from the series dual reporter assay experiments, culminating in Figure 21. When frameshifting occurs, the new reading frame does not contain the downstream GFP gene resulting in a decrease in fluorescence relative to the upstream reporter gene, luciferase. Over the course of 7 experiments, this has been the case where the wildtype G/L has been shown to decrease significantly (with $P < 0.0001$ for the data in Table 2 featuring the average G/L of each experiment) when compared to the mutant construct. An event that knocks out the translation of the plasmid results in neither reporter gene being expressed. This is the value in finding the ratio of the 2 in frame reporter genes: variations in cell count, transfection efficiency, or translation initiation affect both genes evenly. When observing the ratio, the consideration is on the events that affect GFP instead of luciferase, and the design of the construct facilitates this by applying the predicted frameshift site between the two. The potential for internal initiation does exist; however, this would affect both the mutant and the wildtype identically (Pisarev et al., 2005). When comparing the G/L of the mutant and wildtype, there is a significant change that would not be explained by internal initiation, as this process would not select the wildtype over the mutant to a nearly 3-fold degree. This effect can be observed in transfected cells (Figure 20) where mutant cells appear to produce more GFP than the wildtype. While there has been indications of frameshifting at upwards of 80%, most events are relatively sparse (Rodnina et al., 2020) (Atkins et al., 2016). There does exist a potential necessity for a highly efficient frameshift site: the protein sequence that resides in the -1 frame after the frameshift. The 2 geminal UGA codons,

which could be recoded as SeC, would undergo the recoding process only a small percentage of the time, upwards of only 10% (Mehta et al., 2004). Only approximately 1% of the time would both UGAs be recoded, so a highly efficient frameshift would need to occur to allow the production of any reasonable amount of selenoprotein product.

To further enhance the frameshift, the antisense region to DIO2 could recruit a host selenoprotein mRNA to act as a pseudoknot, as well as potentially provide a SECIS element. A single assay has been performed that displays some indication that antisense interactions may enhance frameshifting (Figure 22). Here, the DIO2+ group has an even further reduction G/L compared to the DIO2- group, indicating the rate of frameshifting has increased.

To thoroughly verify that the ATIs enhance frameshifting, future experiments will be performed that feature the GFP in the -1 frame. Currently, there exists the possibility that the ATIs may block translation at the viral insert and prevent the translation of the downstream GFP. Searching for an increase in GFP to verify frameshifting in the presence of antisense sequences would overcome this issue. With the site shown to be functional, if GFP were not expressed in this future construct in the presence of antisense sequences, it would indicate that the ATIs block translation.

CHAPTER V: VIRAL MANIPULATION OF HOST SELENOBIOLOGY

Conclusions

For multiple decades it has been known that viruses, particularly RNA viruses, use our own molecular biology to replicate their genomes during infection—the reverse transcriptase being a principal example wherein this RNA-dependent DNA polymerase converts viral RNA into DNA transcripts, which can be inserted into our own DNA (Boettiger, 1970) (Mizutani et al., 1970) (Lerat & Capy, 1999). The expression of our genome would then result in the replication of the viral sequence therein.

Retroviruses and their ancestors, retrotransposons, have been classic examples of viral manipulation of host biology for decades. Over time, with the advent of several pandemics, we have gained more insight into the mechanisms of how these viruses are able to exploit us, though at great cost. Viruses needed to operate in such a way as to overcome their limited genomic capacities by using the infected host as much as possible. The site of stop codon readthrough and the novel frameshift site shown in Chapters III and IV are examples of condensing genetic information to operate most efficiently. Frameshifting allows for multiple proteins to be encoded in a single gene with multiple overlapping read frames. Stop codon readthrough allows multiple proteins or modules to be expressed without a separate site of initiation. In the case of a UGA stop codon, the inefficiency of the readthrough rate can be advantageous as this can help express a protein at the necessary level relative to the expression of the upstream gene without having excess protein (Mehta et al., 2004). In this way it is similarly beneficial to frameshifting, which also does not occur 100% of the time (Cao & Chen, 2008). The relationship between selenium and viruses is critical to take note of because this element may be targeted by the virus in several ways, both to undermine the host cell and to increase the virulence of the pathogen. Selenium

deficiency has been associated with a number of viral outbreaks, including the recent coronavirus (Beck et al., 2003) (Zhang, Taylor, et al., 2020) (Fakhrolmobasheri et al., 2022).

Viruses have been shown here to possibly target selenoproteins (Figure 11) via mRNA knockdown via ATIs. The sequence complementarity between viral transcripts and host mRNAs is too precise to be coincidental, especially considering the targets. As shown in the gel shift assays from Chapter II (Figures 8-10), the sequences indeed can bind in solution. In the case of the L gene and DIO2 sequences (Figure 10), the shear lane was able to demonstrate the oligonucleotides' ability to find each other and form a duplex despite a multitude of competing sequences. The effect of this interaction has been shown in the knockdown of TR3 at the mRNA level where cellular TR3 mRNA is observed to decrease in SARS-CoV-2 infected cells (Figure 11). A possible rationale for this would be to increase the availability of ribonucleotides for the RNA virus to replicate its genome.

Host selenoproteins may be targeted at the protein level by viral proteases. SARS-CoV-2 M^{pro} may target GPx1, along with several other selenoproteins, to downregulate the DNA synthesis pathway (Gallardo, 2022). This would be a 2-tiered method of increasing ribonucleotides, one at the RNA level and one at the protein level. Proteolysis of selenoproteins leads to oxidative stress and NF- κ B activation, which in turn is responsible for the activation of proinflammatory cytokines (Z. Huang et al., 2012). Increased inflammation because of this can be seen on SARS-CoV-2 infections.

The targeting of selenoproteins may have a broader meaning other than the individual function of the proteins themselves. The possibility of a tethered host mRNA to provide a SECIS element may explain how a virus may encode a selenoprotein without this secondary structure on its RNA. This would be another way for a virus to work with a reduced genome: Use the host

SECIS element, which requires several bases to form, to help encode the viruses UGA codons as SeC. The use of an ATI to provide a secondary structural element may also be found in the functional frameshift site in Ebola virus, where the tethered mRNA may provide the pseudoknot needed to stall frameshifting.

In the NP gene in particular, it is possible that the readthrough product could function as a copper-binding protein, which is vital, as copper ions can be involved in the inactivation of viruses through damage to the envelope, spike proteins, and even the genome (Sagripanti et al., 1997) (Warnes et al., 2015). The UGA at the end of the NP gene is highly conserved in most strains of the virus and features an MXM motif in the translated product that is present in many copper binding proteins (Table S3). Interestingly, the significantly less pathogenic Reston strain of Ebola contains a UAA stop codon at the end of its NP gene (Sappey et al., 1994) (Miranda et al., 1999).

The Ebola L gene frameshift product features 2 geminal UGA codons; this motif is similar to a conserved sequence found in the TXNRD family: -Gly-Cys-SeCys-Gly (Gladyshev et al., 1996). While not evaluated, this frameshift product could serve to perform some redox function. Two tandem SeCs have been shown to be capable of redox activity similar to the Cys-SeCys motif (Shimodaira & Iwaoka, 2019). This protein could help the virus defend itself against antioxidant attacks from the hosts immune system, as well as increase an enveloped virion's survivability intracellularly by inhibiting lipid peroxides.

As a result of viral manipulation of selenobiology, a host's deficiency in selenium would increase the pathogenic effects received. Supplementation of selenium to combat knockdown and proteolysis of selenoproteins would be necessary and has been shown to be effective against symptoms associated with these infections (T.-S. Huang et al., 2013) (Steinbrenner et al., 2015)

(Beck et al., 2004). Selenobiology is often overlooked in virology; however, the viruses themselves deem selenobiology significant enough to target it repeatedly.

REFERENCES

- Advani, V. M., & Dinman, J. D. (2016). Reprogramming the genetic code: The emerging role of ribosomal frameshifting in regulating cellular gene expression. *BioEssays*, 38(1), 21–26. <https://doi.org/10.1002/bies.201500131>
- Atkins, J. F., Loughran, G., Bhatt, P. R., Firth, A. E., & Baranov, P. V. (2016). Ribosomal frameshifting and transcriptional slippage: From genetic steganography and cryptography to adventitious use. *Nucleic Acids Research*, 44(15), 7007–7078. <https://doi.org/10.1093/nar/gkw530>
- Banerjee, A., Kulcsar, K., Misra, V., Frieman, M., & Mossman, K. (2019). Bats and Coronaviruses. *Viruses*, 11(1), 41. <https://doi.org/10.3390/v11010041>
- Beck, M. A., Handy, J., & Levander, O. A. (2004). Host nutritional status: The neglected virulence factor. *Trends in Microbiology*, 12(9), 417–423. <https://doi.org/10.1016/j.tim.2004.07.007>
- Beck, M. A., Levander, O. A., & Handy, J. (2003). Selenium Deficiency and Viral Infection. *The Journal of Nutrition*, 133(5), 1463S–1467S. <https://doi.org/10.1093/jn/133.5.1463S>
- Beck, M. A., Shi, Q., Morris, V. C., & Levander, O. A. (1995). Rapid genomic evolution of a non-virulent Coxsackievirus B3 in selenium-deficient mice results in selection of identical virulent isolates. *Nature Medicine*, 1(5), Article 5. <https://doi.org/10.1038/nm0595-433>
- Bellinger, F. P., Raman, A. V., Reeves, M. A., & Berry, M. J. (2009). Regulation and function of selenoproteins in human disease. *The Biochemical Journal*, 422(1), 11–22. <https://doi.org/10.1042/BJ20090219>

- Bermano, G., Méplan, C., Mercer, D. K., & Hesketh, J. E. (2021). Selenium and viral infection: Are there lessons for COVID-19? *British Journal of Nutrition*, *125*(6), Article 6.
<https://doi.org/10.1017/S0007114520003128>
- Brent, M. R. (2005). Genome annotation past, present, and future: How to define an ORF at each locus. *Genome Research*, *15*(12), 1777–1786. <https://doi.org/10.1101/gr.3866105>
- Brigelius-Flohé, R. (2006). Glutathione peroxidases and redox-regulated transcription factors. *Biological Chemistry*, *387*(10–11), 1329–1335. <https://doi.org/10.1515/BC.2006.166>
- Burk, R. F., Hill, K. E., & Motley, A. K. (2003). Selenoprotein metabolism and function: Evidence for more than one function for selenoprotein P. *The Journal of Nutrition*, *133*(5 Suppl 1), 1517S-20S. <https://doi.org/10.1093/jn/133.5.1517S>
- Cao, S., & Chen, S.-J. (2008). Predicting ribosomal frameshifting efficiency. *Physical Biology*, *5*(1), 16002. <https://doi.org/10.1088/1478-3975/5/1/016002>
- Constans, J., Pellegrin, J.-L., Sergeant, C., Simonoff, M., Pellegrin, I., Fleury, H., Leng, B., & Conri, C. (1995). Serum Selenium Predicts Outcome in HIV Infection: *Journal of Acquired Immune Deficiency Syndromes & Human Retrovirology*, *10*(3), Article 3.
<https://doi.org/10.1097/00042560-199511000-00015>
- Cui, J., Schlub, T. E., & Holmes, E. C. (2014). An Allometric Relationship between the Genome Length and Virion Volume of Viruses. *Journal of Virology*, *88*(11), 6403–6410.
<https://doi.org/10.1128/JVI.00362-14>
- D, B. (1970). RNA-dependent DNA polymerase in virions of RNA tumour viruses. *Nature*, *226*(5252). <https://doi.org/10.1038/2261209a0>
- Dailey, G. P., Premadasa, L. S., Ruzicka, J. A., & Taylor, E. W. (2021). Inhibition of selenoprotein synthesis by Zika virus may contribute to congenital Zika syndrome and

- microcephaly by mimicking SELENOP knockout and the genetic disease PCCA. *BBA Advances*, 1, 100023. <https://doi.org/10.1016/j.bbadv.2021.100023>
- Dietary Supplement Use in the United States, 2003–20061 | Elsevier Enhanced Reader.* (n.d.). <https://doi.org/10.3945/jn.110.133025>
- E. W. Taylor, J. A. Ruzicka, & L. Preamdasa. (2015, May 28). *Translational readthrough of the Ebola nucleoprotein 3'-341 UGA codon via antisense tethering of thioredoxin reductase 3 mRNA*. International342 Congress on Targeting Ebola, Paris, France. <https://doi.org/10.13140/RG.2.2.10237.51683>
- Fakhrolmobasheri, M., Mazaheri-Tehrani, S., Kieliszek, M., Zeinalian, M., Abbasi, M., Karimi, F., & Mozafari, A. M. (2022). COVID-19 and Selenium Deficiency: A Systematic Review. *Biological Trace Element Research*, 200(9), Article 9. <https://doi.org/10.1007/s12011-021-02997-4>
- Fang, L.-Q., Goeijenbier, M., Zuo, S.-Q., Wang, L.-P., Liang, S., Klein, S., Li, X.-L., Liu, K., Liang, L., Gong, P., Glass, G., van Gorp, E., Richardus, J., Ma, J.-Q., Cao, W.-C., & de Vlas, S. (2015). The Association between Hantavirus Infection and Selenium Deficiency in Mainland China. *Viruses*, 7(1), Article 1. <https://doi.org/10.3390/v7010333>
- Feng, Y. X., Yuan, H., Rein, A., & Levin, J. G. (1992). Bipartite signal for read-through suppression in murine leukemia virus mRNA: An eight-nucleotide purine-rich sequence immediately downstream of the gag termination codon followed by an RNA pseudoknot. *Journal of Virology*, 66(8), 5127–5132. <https://doi.org/10.1128/JVI.66.8.5127-5132.1992>
- Gallardo, I. A. (2022). *Identification of SARS-CoV-2 main protease cleavage sites in host cellular selenoproteins and glutathione-related proteins*. The University of North Carolina at Greensboro.

- Gill, H., & Walker, G. (2008). Selenium, immune function and resistance to viral infections. *Nutrition & Dietetics*, 65(s3), S41–S47. <https://doi.org/10.1111/j.1747-0080.2008.00260.x>
- Gladyshev, V. N., Jeang, K. T., & Stadtman, T. C. (1996). Selenocysteine, identified as the penultimate C-terminal residue in human T-cell thioredoxin reductase, corresponds to TGA in the human placental gene. *Proceedings of the National Academy of Sciences of the United States of America*, 93(12), 6146–6151. <https://doi.org/10.1073/pnas.93.12.6146>
- Gonzalez-Flores, J. N., Shetty, S. P., Dubey, A., & Copeland, P. R. (2013). The molecular biology of selenocysteine. *Biomolecular Concepts*, 4(4), 349–365. <https://doi.org/10.1515/bmc-2013-0007>
- Green, L., Kim, C.-H., Bustamante, C., & Tinoco, I. (2008). Characterization of the Mechanical Unfolding of RNA Pseudoknots. *Journal of Molecular Biology*, 375(2), 511–528. <https://doi.org/10.1016/j.jmb.2007.05.058>
- Guillin, O., Vindry, C., Ohlmann, T., & Chavatte, L. (2019). Selenium, Selenoproteins and Viral Infection. *Nutrients*, 11(9), Article 9. <https://doi.org/10.3390/nu11092101>
- Henderson, C. M., Anderson, C. B., & Howard, M. T. (2006). Antisense-induced ribosomal frameshifting. *Nucleic Acids Research*, 34(15), 4302–4310. <https://doi.org/10.1093/nar/gkl531>
- Herring, C. D., & Blattner, F. R. (2004). Global Transcriptional Effects of a Suppressor tRNA and the Inactivation of the Regulator frmR. *Journal of Bacteriology*, 186(20), 6714–6720. <https://doi.org/10.1128/JB.186.20.6714-6720.2004>

- Heyland, D. K., Dhaliwal, R., Suchner, U., & Berger, M. M. (2005). Antioxidant nutrients: A systematic review of trace elements and vitamins in the critically ill patient. *Intensive Care Medicine*, 31(3), 327–337. <https://doi.org/10.1007/s00134-004-2522-z>
- Holmgren, A., & Sengupta, R. (2010). The use of thiols by ribonucleotide reductase. *Free Radical Biology & Medicine*, 49(11), 1617–1628. <https://doi.org/10.1016/j.freeradbiomed.2010.09.005>
- Huang, T.-S., Shyu, Y.-C., Chen, H.-Y., Lin, L.-M., Lo, C.-Y., Yuan, S.-S., & Chen, P.-J. (2013). Effect of parenteral selenium supplementation in critically ill patients: A systematic review and meta-analysis. *PloS One*, 8(1), e54431. <https://doi.org/10.1371/journal.pone.0054431>
- Huang, Z., Rose, A. H., & Hoffmann, P. R. (2012). The role of selenium in inflammation and immunity: From molecular mechanisms to therapeutic opportunities. *Antioxidants & Redox Signaling*, 16(7), 705–743. <https://doi.org/10.1089/ars.2011.4145>
- Israël, N., Gougerot-Pocidallo, M. A., Aillet, F., & Virelizier, J. L. (1992). Redox status of cells influences constitutive or induced NF-kappa B translocation and HIV long terminal repeat activity in human T and monocytic cell lines. *The Journal of Immunology*, 149(10), 3386–3393. <https://doi.org/10.4049/jimmunol.149.10.3386>
- Jacks, T., Madhani, H. D., Masiarz, F. R., & Varmus, H. E. (1988). Signals for ribosomal frameshifting in the Rous sarcoma virus gag-pol region. *Cell*, 55(3), 447–458. [https://doi.org/10.1016/0092-8674\(88\)90031-1](https://doi.org/10.1016/0092-8674(88)90031-1)
- Jacks, T., Power, M. D., Masiarz, F. R., Luciw, P. A., Barr, P. J., & Varmus, H. E. (1988). Characterization of ribosomal frameshifting in HIV-1 gag-pol expression. *Nature*, 331(6153), Article 6153. <https://doi.org/10.1038/331280a0>

- Lei, L., Cheng, A., Wang, M., & Jia, R. (2022). The Influence of Host miRNA Binding to RNA Within RNA Viruses on Virus Multiplication. *Frontiers in Cellular and Infection Microbiology*, *12*, 802149. <https://doi.org/10.3389/fcimb.2022.802149>
- Lerat, E., & Capy, P. (1999). Retrotransposons and retroviruses: Analysis of the envelope gene. *Molecular Biology and Evolution*, *16*(9), 1198–1207. <https://doi.org/10.1093/oxfordjournals.molbev.a026210>
- Lin, Z., Gilbert, R. J. C., & Brierley, I. (2012). Spacer-length dependence of programmed –1 or –2 ribosomal frameshifting on a U6A heptamer supports a role for messenger RNA (mRNA) tension in frameshifting. *Nucleic Acids Research*, *40*(17), 8674–8689. <https://doi.org/10.1093/nar/gks629>
- Lipinski, B. (2015). Can Selenite be an Ultimate Inhibitor of Ebola and Other Viral Infections? *British Journal of Medicine and Medical Research*, *6*, 319–324. <https://doi.org/10.9734/BJMMR/2015/14858>
- Luongo, C., Dentice, M., & Salvatore, D. (2019). Deiodinases and their intricate role in thyroid hormone homeostasis. *Nature Reviews. Endocrinology*, *15*(8), 479–488. <https://doi.org/10.1038/s41574-019-0218-2>
- Mehta, A., Rebsch, C. M., Kinzy, S. A., Fletcher, J. E., & Copeland, P. R. (2004). Efficiency of Mammalian Selenocysteine Incorporation *. *Journal of Biological Chemistry*, *279*(36), 37852–37859. <https://doi.org/10.1074/jbc.M404639200>
- Miranda, M. E., Ksiazek, T. G., Retuya, T. J., Khan, A. S., Sanchez, A., Fulhorst, C. F., Rollin, P. E., Calaor, A. B., Manalo, D. L., Roces, M. C., Dayrit, M. M., & Peters, C. J. (1999). Epidemiology of Ebola (subtype Reston) virus in the Philippines, 1996. *The Journal of Infectious Diseases*, *179 Suppl 1*, S115-119. <https://doi.org/10.1086/514314>

- Molteni, C. G., Principi, N., & Esposito, S. (2014). Reactive oxygen and nitrogen species during viral infections. *Free Radical Research*, *48*(10), 1163–1169.
<https://doi.org/10.3109/10715762.2014.945443>
- Nelson, H. K., Shi, Q., Van Dael, P., Schiffrin, E. J., Blum, S., Barclay, D., Levander, O. A., & Beck, M. A. (2001). Host nutritional selenium status as a driving force for influenza virus mutations. *The FASEB Journal*, *15*(10), 1727–1738. <https://doi.org/10.1096/fj.01-0108com>
- Olubajo, B., & Taylor, E. W. (2005). A -1 frameshift in the HIV-1 env gene is enhanced by arginine deficiency via a hungry codon mechanism. *Mutation Research*, *579*(1–2), 125–132. <https://doi.org/10.1016/j.mrfmmm.2005.02.018>
- Pisarev, A. V., Shirokikh, N. E., & Hellen, C. U. T. (2005). Translation initiation by factor-independent binding of eukaryotic ribosomes to internal ribosomal entry sites. *Comptes Rendus Biologies*, *328*(7), 589–605. <https://doi.org/10.1016/j.crv.2005.02.004>
- Rayman, M. P., Taylor, E. W., & Zhang, J. (2022). The relevance of selenium to viral disease with special reference to SARS-CoV-2 and COVID-19. *Proceedings of the Nutrition Society*, 1–12. <https://doi.org/10.1017/S0029665122002646>
- Rehmsmeier, M., Steffen, P., Hochsmann, M., & Giegerich, R. (2004). Fast and effective prediction of microRNA/target duplexes. *RNA (New York, N.Y.)*, *10*(10), 1507–1517.
<https://doi.org/10.1261/rna.5248604>
- Rodnina, M. V., Korniy, N., Klimova, M., Karki, P., Peng, B.-Z., Senyushkina, T., Belardinelli, R., Maracci, C., Wohlgemuth, I., Samatova, E., & Peske, F. (2020). Translational recoding: Canonical translation mechanisms reinterpreted. *Nucleic Acids Research*, *48*(3), 1056–1067. <https://doi.org/10.1093/nar/gkz783>

- Rogers, E. J., Ambulos, N. P., & Lovett, P. S. (1991). Ribosome hopping and translational frameshifting are inadequate alternatives to translational attenuation in cat-86 regulation. *Journal of Bacteriology*, *173*(24), 7881–7886. <https://doi.org/10.1128/jb.173.24.7881-7886.1991>
- S, M., D, B., & Hm, T. (1970). A DNA-dependent DNA polymerase and a DNA endonuclease in virions of Rous sarcoma virus. *Nature*, *228*(5270). <https://doi.org/10.1038/228424a0>
- Sagripanti, J. L., Routson, L. B., Bonifacino, A. C., & Lytle, C. D. (1997). Mechanism of copper-mediated inactivation of herpes simplex virus. *Antimicrobial Agents and Chemotherapy*, *41*(4), 812–817. <https://doi.org/10.1128/AAC.41.4.812>
- Saito, Y., & Takahashi, K. (2002). Characterization of selenoprotein P as a selenium supply protein. *European Journal of Biochemistry*, *269*(22), 5746–5751. <https://doi.org/10.1046/j.1432-1033.2002.03298.x>
- Sappey, C., Legrand-Poels, S., Best-Belpomme, M., Favier, A., Rentier, B., & Piette, J. (1994). Stimulation of glutathione peroxidase activity decreases HIV type 1 activation after oxidative stress. *AIDS Research and Human Retroviruses*, *10*(11), 1451–1461. <https://doi.org/10.1089/aid.1994.10.1451>
- Shimodaira, S., & Iwaoka, M. (2019). Synthesis of selenocysteine-containing dipeptides modeling the active site of thioredoxin reductase. *Phosphorus, Sulfur, and Silicon and the Related Elements*, *194*(7), 750–752. <https://doi.org/10.1080/10426507.2019.1603721>
- Skalsky, R. L., & Cullen, B. R. (2010). Viruses, microRNAs, and Host Interactions. *Annual Review of Microbiology*, *64*, 123–141. <https://doi.org/10.1146/annurev.micro.112408.134243>

- Steinbrenner, H., Al-Quraishy, S., Dkhil, M. A., Wunderlich, F., & Sies, H. (2015). Dietary Selenium in Adjuvant Therapy of Viral and Bacterial Infections. *Advances in Nutrition*, 6(1), Article 1. <https://doi.org/10.3945/an.114.007575>
- Stýblo, M., Walton, F. S., Harmon, A. W., Sheridan, P. A., & Beck, M. A. (2007). Activation of superoxide dismutase in selenium-deficient mice infected with influenza virus. *Journal of Trace Elements in Medicine and Biology*, 21(1), 52–62. <https://doi.org/10.1016/j.jtemb.2006.11.001>
- Taylor, E. W. (2020). *RNA Viruses vs. DNA Synthesis: A General Viral Strategy That May Contribute to the Protective Antiviral Effects of Selenium*. <https://doi.org/10.20944/preprints202006.0069.v1>
- Taylor, E. W., Ruzicka, J. A., Premadasa, L., & Zhao, L. (2016). Cellular Selenoprotein mRNA Tethering via Antisense Interactions with Ebola and HIV-1 mRNAs May Impact Host Selenium Biochemistry. *Current Topics in Medicinal Chemistry*, 16(13), Article 13. <https://doi.org/10.2174/1568026615666150915121633>
- Theis, C., Reeder, J., & Giegerich, R. (2008). KnotInFrame: Prediction of -1 ribosomal frameshift events. *Nucleic Acids Research*, 36(18), 6013–6020. <https://doi.org/10.1093/nar/gkn578>
- Turanov, A. A., Everley, R. A., Hybsier, S., Renko, K., Schomburg, L., Gygi, S. P., Hatfield, D. L., & Gladyshev, V. N. (2015). Regulation of Selenocysteine Content of Human Selenoprotein P by Dietary Selenium and Insertion of Cysteine in Place of Selenocysteine. *PloS One*, 10(10), e0140353. <https://doi.org/10.1371/journal.pone.0140353>

- Wang, Y., Huang, J., Sun, Y., Stubbs, D., He, J., Li, W., Wang, F., Liu, Z., Ruzicka, J. A., Taylor, E. W., Rayman, M. P., Wan, X., & Zhang, J. (2021). SARS-CoV-2 suppresses mRNA expression of selenoproteins associated with ferroptosis, endoplasmic reticulum stress and DNA synthesis. *Food and Chemical Toxicology*, *153*, 112286.
<https://doi.org/10.1016/j.fct.2021.112286>
- Warnes, S. L., Little, Z. R., & Keevil, C. W. (2015). Human Coronavirus 229E Remains Infectious on Common Touch Surface Materials. *MBio*, *6*(6), e01697-15.
<https://doi.org/10.1128/mBio.01697-15>
- Will Taylor, E., A. Ruzicka, J., Premadasa, L., & Zhao, L. (2016). Cellular Selenoprotein mRNA Tethering via Antisense Interactions with Ebola and HIV-1 mRNAs May Impact Host Selenium Biochemistry. *Current Topics in Medicinal Chemistry*, *16*(13), Article 13.
<https://doi.org/10.2174/1568026615666150915121633>
- Winkel, L. H. E., Vriens, B., Jones, G. D., Schneider, L. S., Pilon-Smits, E., & Bañuelos, G. S. (2015). Selenium cycling across soil-plant-atmosphere interfaces: A critical review. *Nutrients*, *7*(6), 4199–4239. <https://doi.org/10.3390/nu7064199>
- Yoshioka, J. (2015). Thioredoxin Reductase 2 (Txnrd2) Regulates Mitochondrial Integrity in the Progression of Age-Related Heart Failure. *Journal of the American Heart Association*, *4*(7), e002278. <https://doi.org/10.1161/JAHA.115.002278>
- Yu Yu, S., Zhu, Y. J., & Li, W. G. (1997). Protective role of selenium against hepatitis B virus and primary liver cancer in Qidong. *Biological Trace Element Research*, *56*(1), Article 1.
<https://doi.org/10.1007/BF02778987>
- Zeng, Y., Yi, R., & Cullen, B. R. (2003). MicroRNAs and small interfering RNAs can inhibit mRNA expression by similar mechanisms. *Proceedings of the National Academy of*

Sciences of the United States of America, 100(17), 9779–9784.

<https://doi.org/10.1073/pnas.16307971100>

Zhang, J., Saad, R., Taylor, E. W., & Rayman, M. P. (2020). Selenium and selenoproteins in viral infection with potential relevance to COVID-19. *Redox Biology*, 37, 101715.

<https://doi.org/10.1016/j.redox.2020.101715>

Zhang, J., Taylor, E. W., Bennett, K., Saad, R., & Rayman, M. P. (2020). Association between regional selenium status and reported outcome of COVID-19 cases in China. *The American Journal of Clinical Nutrition*, 111(6), Article 6.

<https://doi.org/10.1093/ajcn/nqaa095>

Zhao, L., Cox, A. G., Ruzicka, J. A., Bhat, A. A., Zhang, W., & Taylor, E. W. (2000). Molecular modeling and *in vitro* activity of an HIV-1-encoded glutathione peroxidase. *Proceedings of the National Academy of Sciences*, 97(12), Article 12.

<https://doi.org/10.1073/pnas.97.12.6356>

Zhao, L., Olubajo, B., & Taylor, E. W. (2006). Functional studies of an HIV-1 encoded glutathione peroxidase. *BioFactors (Oxford, England)*, 27(1–4), 93–107.

<https://doi.org/10.1002/biof.5520270109>

Figure A23. Initial Construct Design Featuring Secreted Alkaline Phosphatase Upstream of the Potential Frameshift Insert

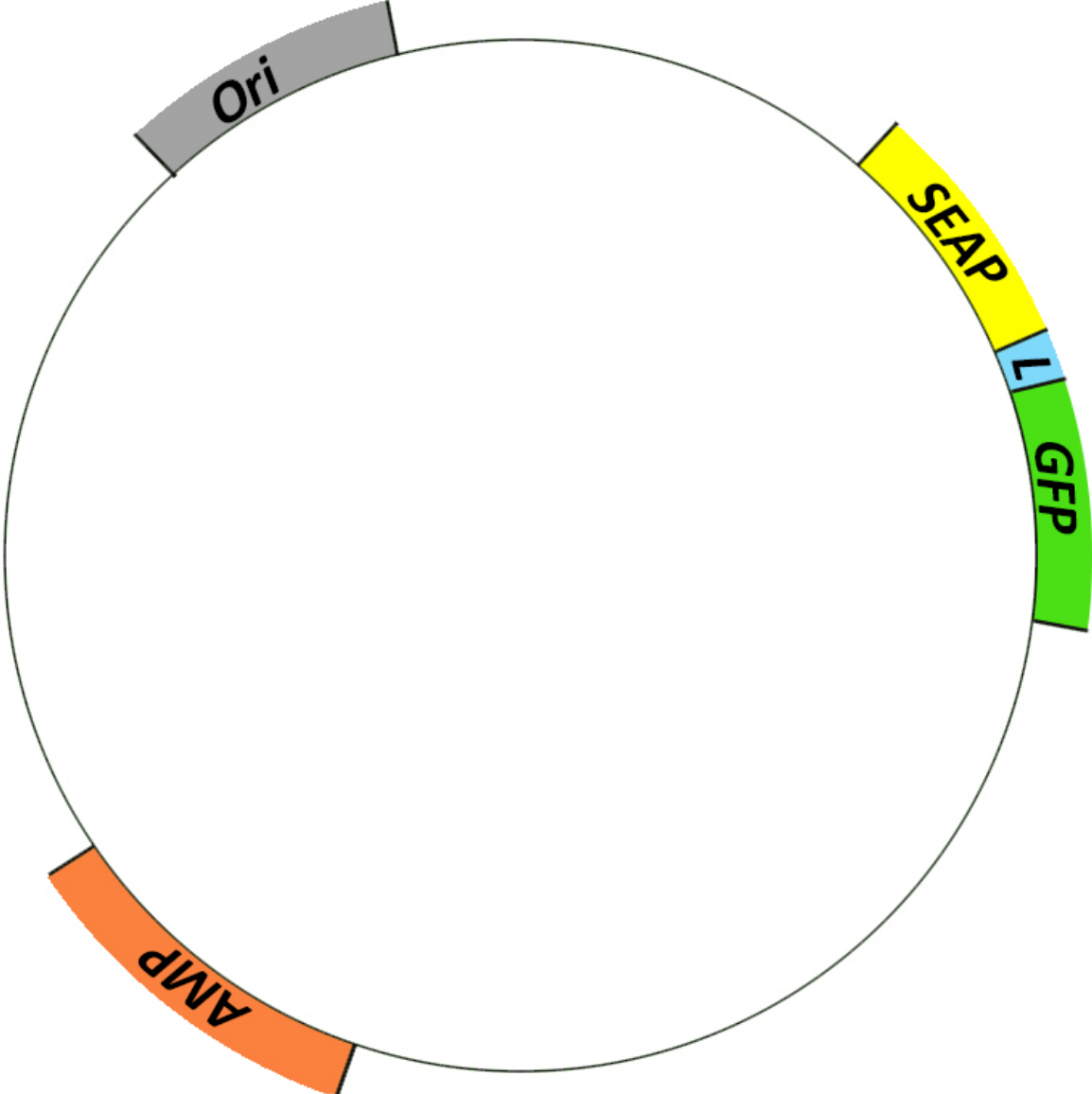


Table A3. Sets A-G**Set A**

GFP	1	2	3	4	5
Control	6207.3	6761.8	5432	6210	5285
Mutant	5866.9	7043.9	5841.2	6339.7	5956.7
Wildtype	32296	16053	12867	11402	15407

Luciferase	1	2	3	4	5
Control	114.64	-59.74	-16.9	0.865	0.096
Mutant	184.88	10.616	43.616	112.33	112.09
Wildtype	477.26	3110	936.13	63.644	343.1

G:L	1	2	3	4	5
Control	54.1460223	-113.18714	-321.42012	7179.19075	55052.0833
Mutant	31.7335569	663.517332	133.923331	56.4381732	53.1421179
Wildtype	67.669614	5.16173633	13.7448859	179.152787	44.9052754

	Average	SEM
Control	12370.1626	9627.64167
Mutant	187.750902	107.509083
Wildtype	62.1268598	28.0058662

Set B

GFP	1	2	3	4	5
Mutant	5828	6310	5808	57190	116008
Wild	40792	12867	8181	6585	9967
Control	5654	6177	5379	5865	7045

Luciferase	1	2	3	4	5
Mutant	62.6	42.1	39	1007	1089
Wild	834.5	667.8	240.6	316.7	268
Control	63.5	134.7	19.1	64.8	99.6

G:L	1	2	3	4	5
Mutant	93.0990415	149.881235	148.923077	56.7924528	106.527089
Wild	48.8819652	19.2677448	34.0024938	20.7925482	37.1902985
Control	89.0393701	45.857461	281.623037	90.5092593	70.7329317

	Average	SEM
Mutant	111.044579	17.6476765
Wild	32.0270101	5.49392201
Control	115.552412	42.2940452

Set C

GFP	1	2	3	4	5
Control	14537	11127	11172	10843	13649
Mutant	16911	14147	12423		
Wildtype	15992	13242	18551	15998	16745

Luciferase	1	2	3	4	5
Control	82	-37.4	75.6	51.2	27.3
Mutant	297.66	507.86	627.84		
Wildtype	2054	708.5	1503.6	2625.7	780.3

G:L	1	2	3	4	5
Control	177.280488	-297.51337	147.777778	211.777344	499.96337
Mutant	56.8131425	27.8561021	19.7868884		
Wildtype	7.78578384	18.6901905	12.3377228	6.09285143	21.459695

	Average	SEM
Control	147.857122	127.922871
Mutant	34.818711	8.70740278
Wildtype	12.9378991	3.16210268

Set D

GFP	1	2	3	4	5
Control	8854	9570	7923	9181	7424
Mutant	8096	8691			
Wildtype	10472	11746	10155	10514	

Luciferase	1	2	3	4	5
Control	-87	-12	-4	-53	-41
Mutant	15	60			
Wildtype	157.8	112.8	172.3	112.27	

G:L	1	2	3	4	5
Control	-101.77011	-797.5	-1980.75	-173.22642	-181.07317
Mutant	539.733333	144.85			
Wildtype	66.3624842	104.131206	58.937899	93.6492384	

	Average	SEM
Control	-646.86394	356.396133
Mutant	342.291667	197.441667
Wildtype	80.7702068	10.7851667

Set E

GFP	1	2	3
Control	5955	5872	5344
Mutant	9286	9663	9611
Wildtype	11505	10653	9928

Luciferase	1	2	3
Control	-14.29	17.485	7.038
Mutant	324.72	603.69	285.3
Wildtype	1733.8	1463.8	796.05

G:L	1	2	3
Control	-416.72498	335.830712	759.306621
Mutant	28.5969451	16.0065597	33.6873467
Wildtype	6.63571346	7.27763356	12.4715784

	Average	SEM
Control	226.13745	343.89293
Mutant	26.0969505	5.25484021
Wildtype	8.79497515	1.84761775

Set F

GFP	1	2	3	4	5	6
Control	10275	11439	11411	10911	10329	9547
Mutant	15166	14479	15882	14849	13333	13787
Wildtype	21571	20114	14611	15050	20755	24013

Luciferase	1	2	3	4	5	6
Control	-41	-79	-151	-116	-123	-80
Mutant	104.83	153.07	109.01	290.25	101.84	215.94
Wildtype	713.91	676.42	333.94	362.8	651.56	1044

G:L	1	2	3	4	5	6
Control	-250.60976	-144.79747	-75.569536	-94.060345	-83.97561	-119.3375
Mutant	144.67232	94.590710	145.69305	51.159345	130.92105	63.846438
Wildtype	30.215293	29.735962	43.753368	41.4829107	31.8543189	23.0009579

	Average	SEM
Control	-128.05837	26.6015829
Mutant	105.147155	16.9335705
Wildtype	33.3404687	3.19687953

Set G

GFP	1	2	3
Control	8133	9849	11588
Mutant	131242	48161	62758
Wildtype	31665	24735	40258

Luciferase	1	2	3
Control	-50.3	85.7	-3.2
Mutant	1135	921	898
Wildtype	423	416	767

G:L	1	2	3
Control	-161.68986	114.924154	-3621.25
Mutant	115.631718	52.2920738	69.8864143
Wildtype	74.858156	59.4591346	52.487614

	Average	SEM
Control	-1222.6719	1201.94447
Mutant	79.2700687	18.8769468
Wildtype	62.2683016	6.6088035

Note: Transfection Assay Raw Data: Seven separate experiments A-G, measuring the signal from Green Fluorescent Protein and Luciferase, the ratio of the 2 signals as G/L and the averages of each set, along with the SEM.

Table A4. Antisense Induction of Frameshifting

GFP	1	2	3	4	5
DIO2-	9690	10698	11658	12780	10036
DIO2+	47386	19472	8635	12256	8683
Luc					
DIO2-	129.14	127.12	67.163	124.46	144
DIO2+	144.36	129.35	43.895	144.96	140.89
G/L					
DIO2-	75.0348459	84.1567023	173.577714	102.683593	669.265109
DIO2+	328.248822	150.537302	196.719444	84.5474614	66.21
GFP	6	7	8	9	10
DIO2-	11360	20767	49023	66001	29728
DIO2+	41876				
Luc					
DIO2-	60.9	86.554	73.249	37.528	76.054
DIO2+	104.71				
G/L					
DIO2-	186.535304	239.931141	669.265109	1758.71349	390.880164
DIO2+	94.73				

	Average	SEM
DIO2-	388.336931	152.054726
DIO2+	153.498838	51.5068196

	Ratio of GFP to Luciferase	SEM
DIO2-	2.52990144	0.99059203
DIO2+	1	0.33555185

Note: Transfection Assay Raw Data: A single experiment measuring the signal from green fluorescent protein and luciferase, the ratio of the 2 signals as G/L and the average, along with the SEM. The normalized data are included as well.

Table A5. Amino Acid Sequence Homology of Copper Binding Proteins

Multicopper oxidase [Acinetobacter gernerii]

Query 1 QHHQUMSM 8

QHHQ MSM

Sbjct 384 QHHQSMSM 391

Multicopper oxidase [Acinetobacter gernerii]

Query 1 QHHQUMSM 8

QHHQ MSM

Sbjct 384 QHHQSMSM 391

copper-transporting ATPase 1 [Tupaia chinensis]

Query 1 QHHQUMSMEQ 10

+H Q MSME+

Sbjct 682 HHNQSMSMEE 691

copper resistance protein B, partial [Acinetobacter indicus]

Query 1 QHHQUMSM 8

Q+HQ MSM

Sbjct 23 QQHQLMSM 30

copper oxidase [Ruegeria pomeroyi]

Query 2 HHQCMSMEQ 10

H +CM MEQ

Sbjct 128 HPHCMTMEQ 136

Figure A24. IntaRNA Results of DIO2 and Ebola L Gene From Figure 10

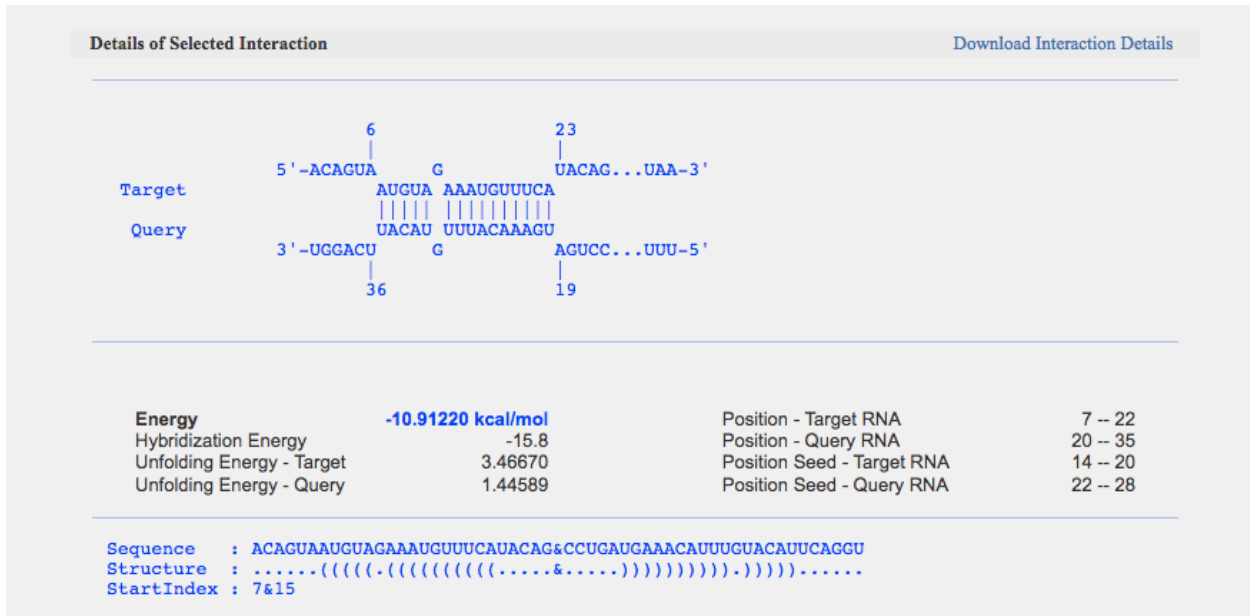


Figure A25. IntaRNA Results of SARS-CoV-2 and Fruit Bat TR3 From Figure 9

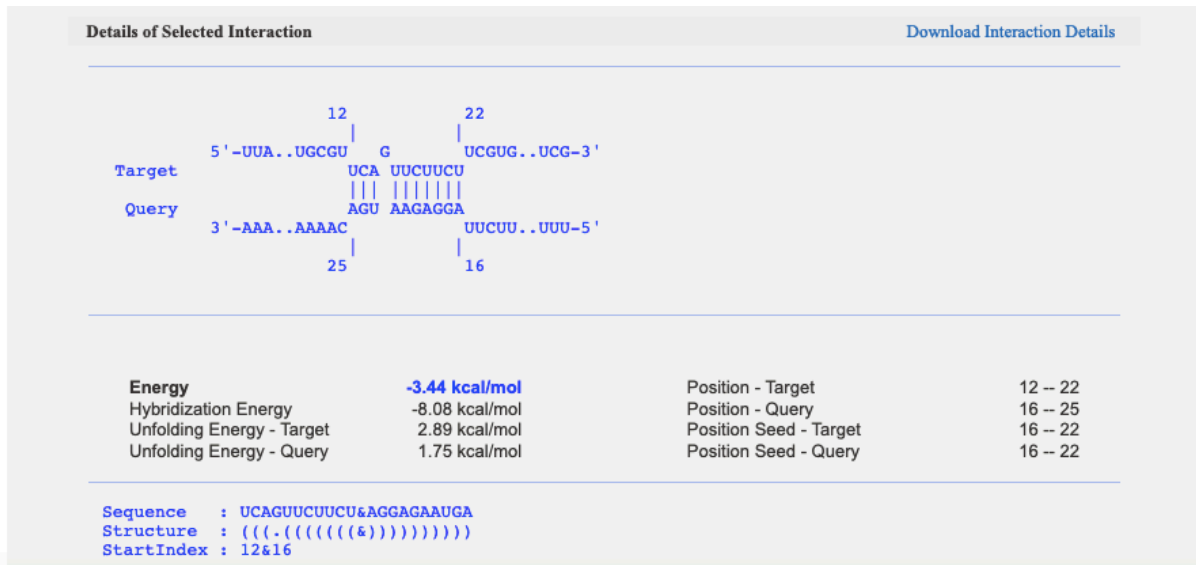


Figure A26. IntraRNA Results of SARS-CoV-2 and Human TR3 From Figure 8B.

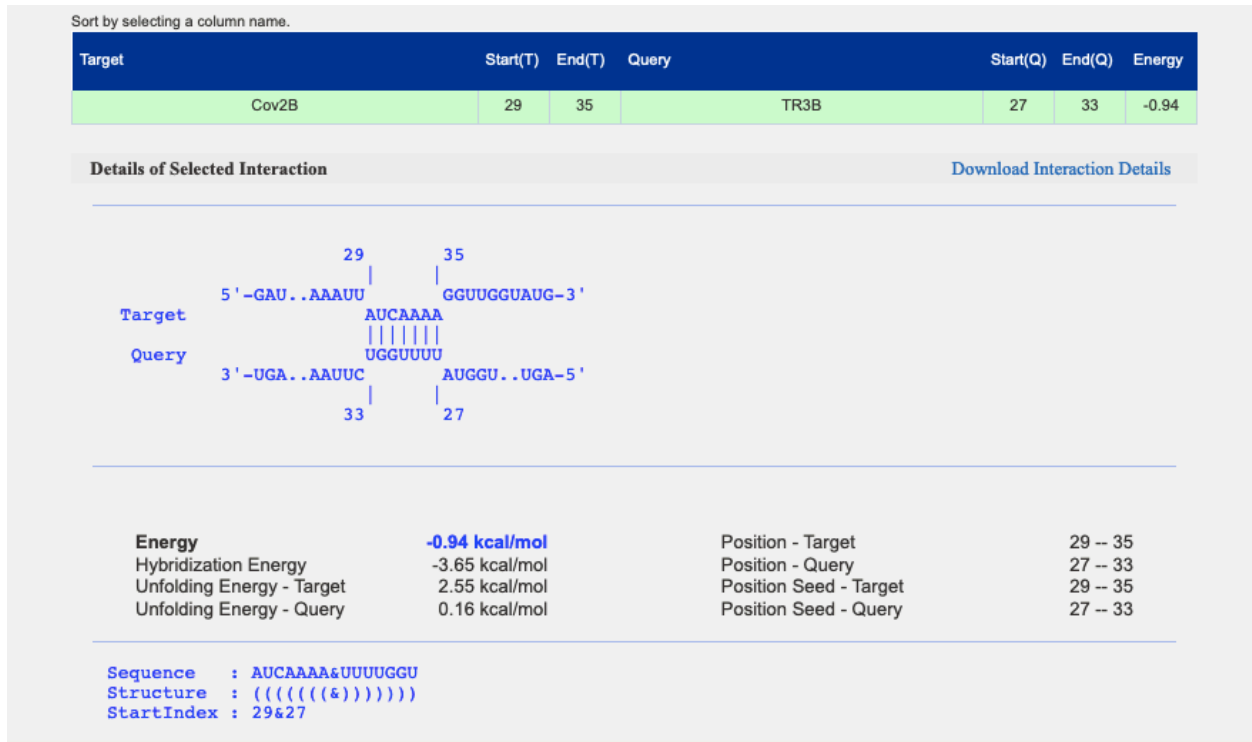


Figure A27. RNAStructure Results of Ebola L Gene Oligo Used in Figure 10

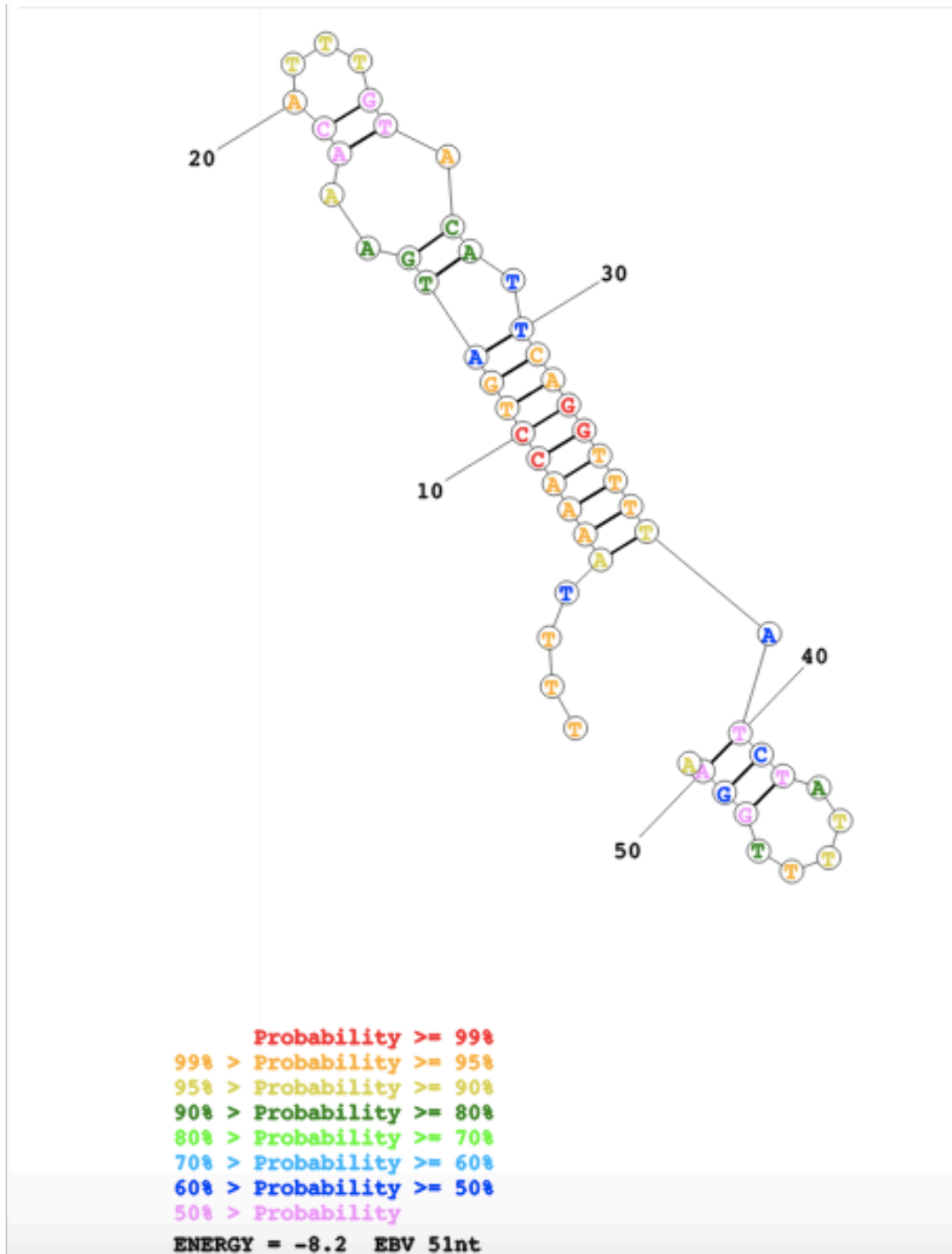
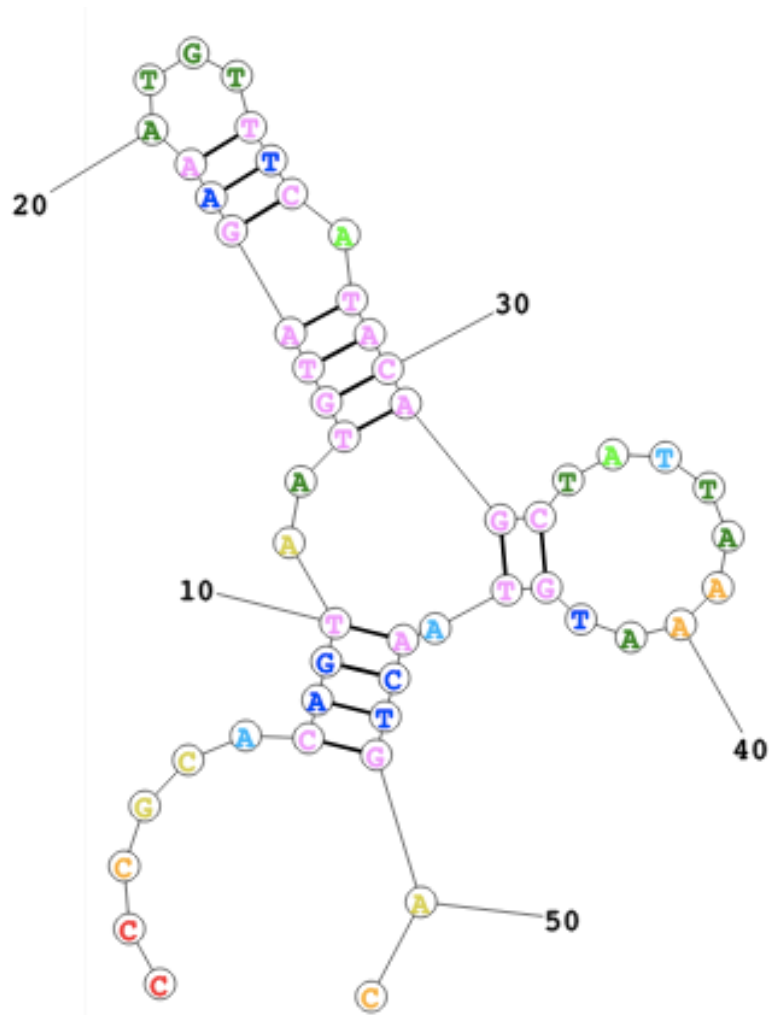


Figure A28. RNAStructure Results of DIO2 Used in Figure 10



Probability >= 99%
99% > Probability >= 95%
95% > Probability >= 90%
90% > Probability >= 80%
80% > Probability >= 70%
70% > Probability >= 60%
60% > Probability >= 50%
50% > Probability

ENERGY = -2.2 DIO 51nt

Figure A29. RNAStructure Results of Human TR3 Oligo Used in Figure 8

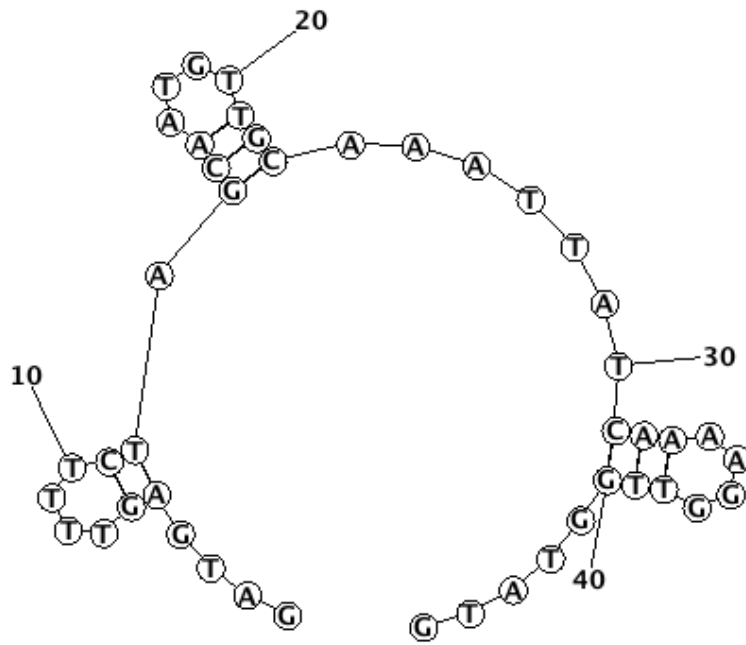


Figure A30. RNAStructure Results of SARS-CoV-2 Oligo Used in Figure 9

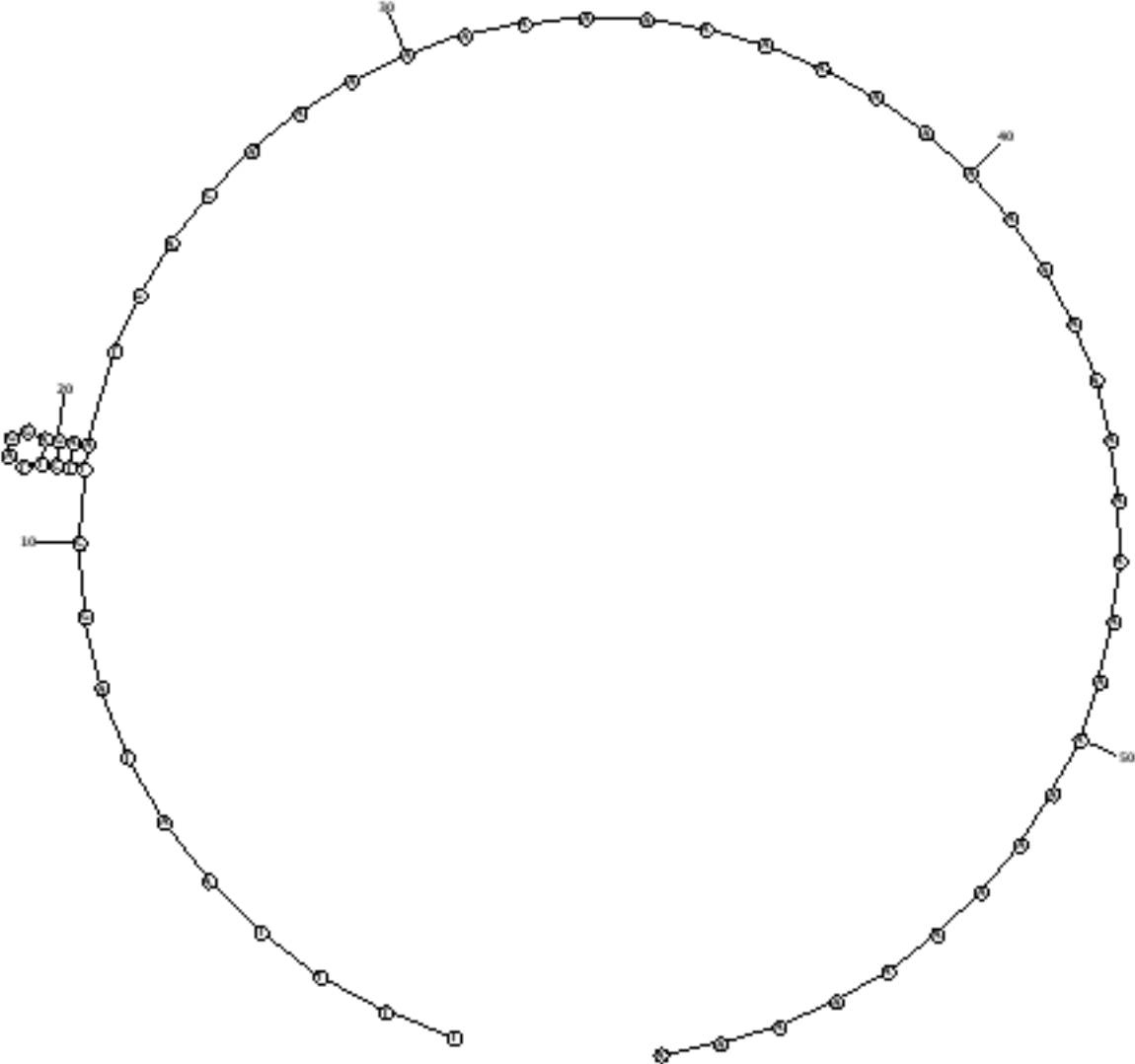
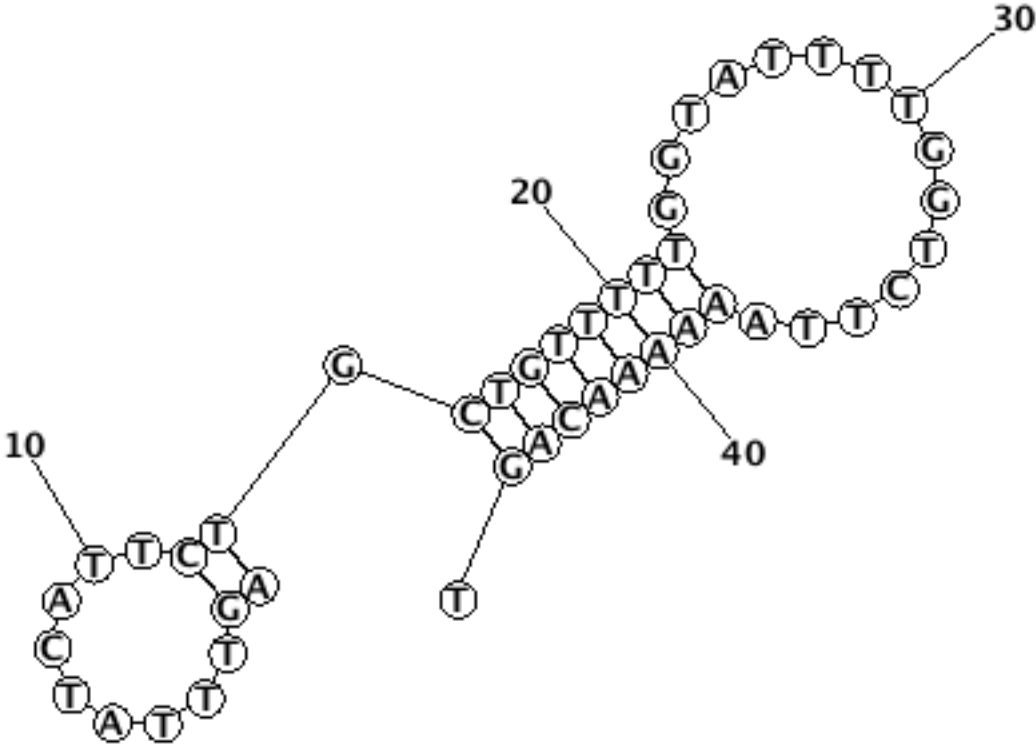


Figure A31. RNAStructure Results of SARS-CoV-2 Oligo Used in Figure 8



4

Figure A33. Raw Uncropped Gel of Figure 8

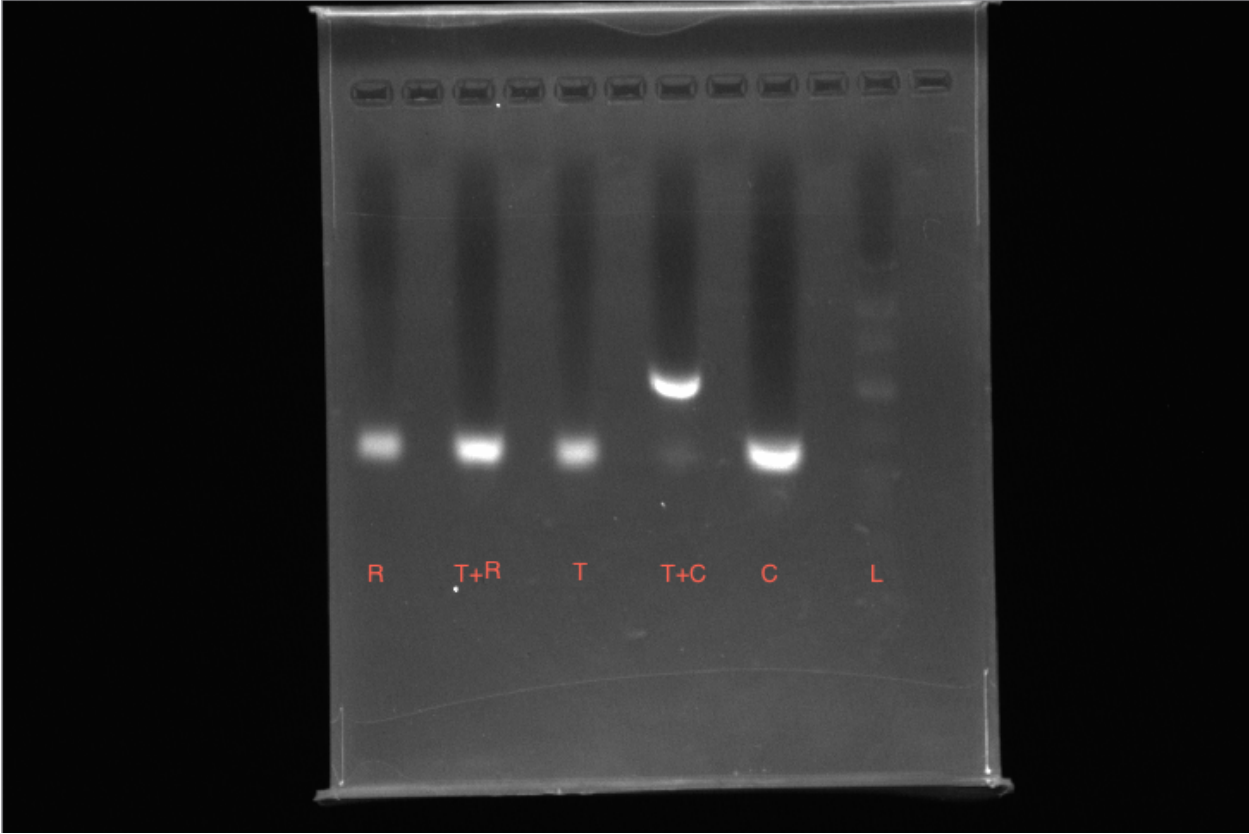


Figure A34. Raw Uncropped Gel of Figure 9

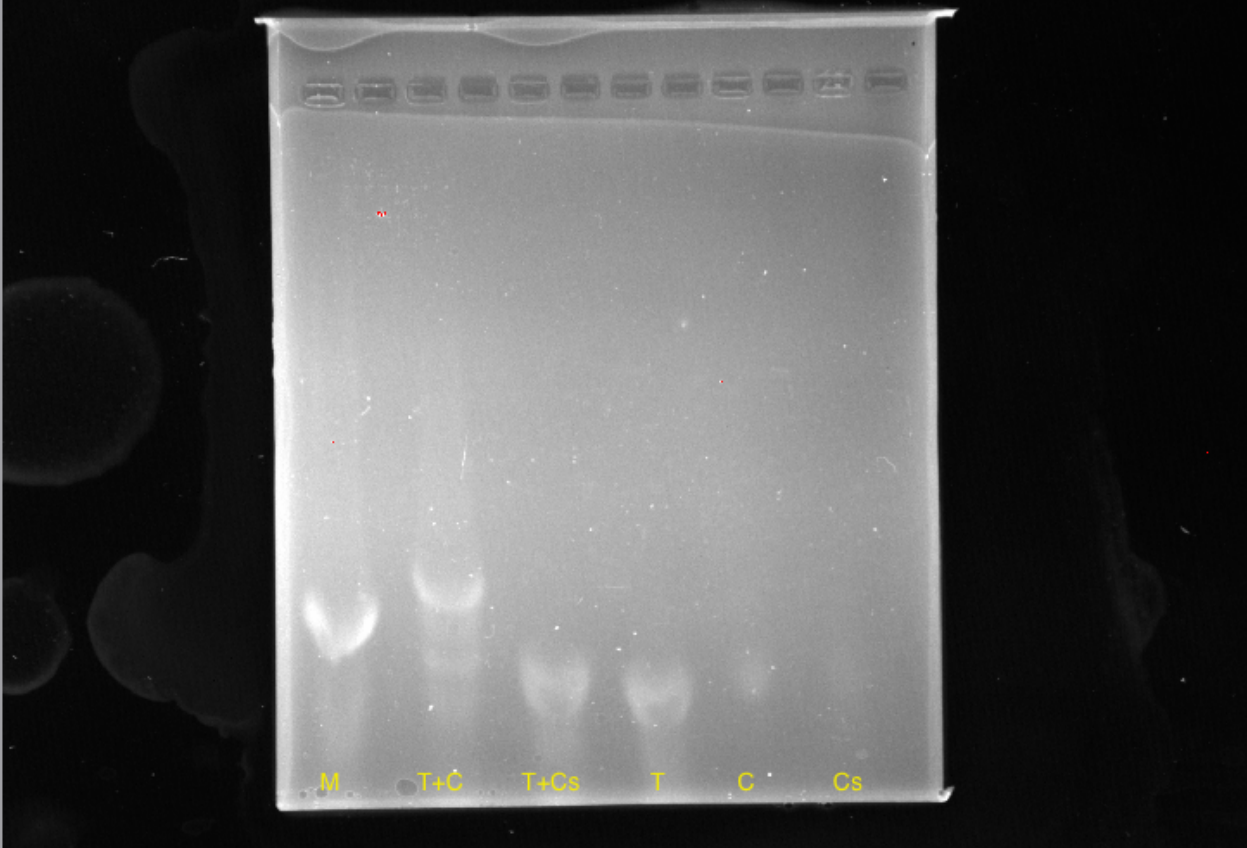
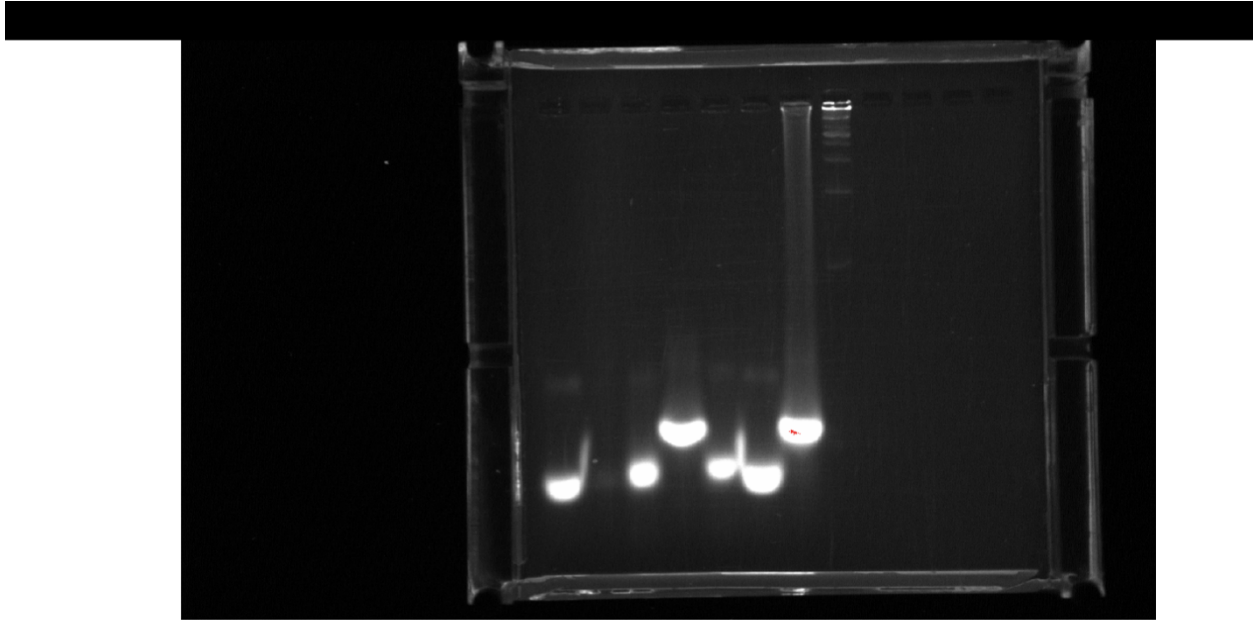


Figure A35. Raw Uncropped Gel of Figure 10



DIO EBV SCR D+E D+S E+S D+E+Shear Ladder